DEGREE PROJECT

Stochastic Optimal Trajectory Generation via Multivariate Polynomial Chaos

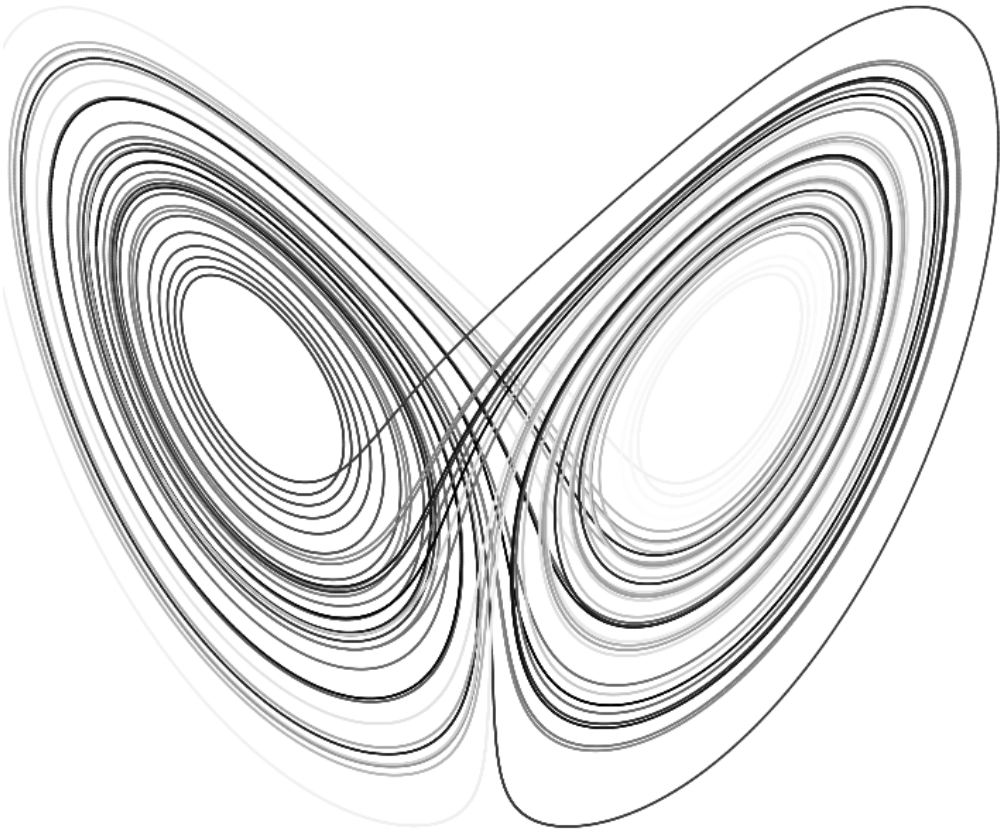

Lisa Whittle

Space Engineering, master's level (120 credits)
2017

Luleå University of Technology
Department of Computer Science, Electrical and Space Engineering

LULEÅ UNIVERSITY OF TECHNOLOGY

MASTER'S THESIS

Stochastic Optimal Trajectory Generation via Multivariate Polynomial Chaos

Author:
Lisa Whittle

Supervisor:
Dr. Marco Sagliano

A thesis undertaken within:

GNC department
Institute of Space Systems
Deutsches Zentrum für Luft- und Raumfahrt (DLR), Bremen, Germany

Submitted in partial fulfillment of the requirements for the programme of:

Master Techniques Spatiales et Instrumentation
Faculté Sciences et Ingénierie
Université Paul Sabatier - Toulouse III

as part of the
Joint European Master in Space Science and Technology (SpaceMaster)

25th August 2017

Université Paul Sabatier - Toulouse III

Abstract

Faculté Sciences et Ingénierie

Master Techniques Spatiales et Instrumentation

Stochastic Optimal Trajectory Generation via Multivariate Polynomial Chaos

by **Lisa Whittle**

This thesis presents a framework that has been developed in order to compute stochastic optimal trajectories. This is achieved by transforming the initial set of stochastic ordinary differential equations into their deterministic equivalent by application of Multivariate Polynomial Chaos. Via Galerkin projection, it is possible to include stochastic information in the optimal-trajectory generation process, and to solve the corresponding optimal-control problem using pseudospectral methods. The resultant trajectory is therefore less sensitive to the uncertainties included in the analysis, e.g., those present in system parameters, initial conditions or path constraints. The accurate, yet computationally efficient manner in which solutions are obtained is presented and a comparison with deterministic results show the benefits of the proposed approach for a variety of numerical examples.

Acknowledgements

I would like to thank everyone within the GNC department at the DLR Institute of Space Systems for making my time here so enjoyable and insightful. I am of course particularly grateful to my supervisor Dr. Marco Sagliano who has been incredibly supportive and inspiring throughout. He not only introduced me to this brilliant topic, but has also given me a greater comprehension and appreciation of the GNC field.

Special mention also goes to everyone involved in the SpaceMaster (ERASMUS+) programme, as the last two years have without a doubt been the best of my life. From the first days in Würzburg, to Kiruna and then Toulouse, I have met some incredible people during this time; all whilst studying something I love.

Most importantly, I am thankful for my family and friends, who have encouraged me every step of the way and who continue to make each day brighter, no matter the distance between us.

Contents

List of Figures

List of Tables

List of Abbreviations

AOCP	Augmented Optimal Control Problem
DLR	Deutsches Zentrum für Luft- und Raumfahrt
EDL	Entry Descent and Landing
EKF	Extended Kalman Filter
gPC	Generalised Polynomial Chaos
LTI	Linear Time Invariant
MC	Monte Carlo
MPBVP	Multiple-Point Boundary-Value Problem
NLP	Nonlinear Programming
OCP	Optimal Control Problem
ODE	Ordinary Differential Equation
PC	Polynomial Chaos
PCE	Polynomial Chaos Expansion
PDF	Probability Density Function
PS	Pseudospectral
SPARTAN	SHEFEX-3 Pseudospectral Algorithm for Reentry Trajectory ANalysis
UQ	Uncertainty Quantification
UKF	Unscented Kalman Filtering

List of Symbols

Roman		
A	Augmented matrix for state	
B	Augmented matrix for control	
a_i	Initial parameter coefficients	
d	Number of independent random variables	
e_{ijk}	Integral of triple polynomial product	
F	Probability density function	
g	Path constraint	
J	Cost function	
$\mathcal{L}_2$	Norm space	
l_b	Lower bound for uniform distribution	
n	Order of polynomial expansion	
P	Order of problem	
t	Time	s
t_0	Initial time	s
t_f	Final time	s
u	Control	
u^*	Optimal Control	
u_b	Upper bound for uniform distribution	
W	Weights from inner products	
x	States	
x_0	Initial states	
Greek		
α	Multi index	
ξ	Random variable	
γ	Normalization factor	
μ	Statistical mean	
μ_a	Mean of parameter	
μ_x	Mean of initial condition	
τ	Pseudospectral domain	
σ	Statistical standard deviation	
σ_a	Standard deviation of parameter	
σ_x	Standard deviation of initial condition	
σ^2	Variance	
ψ	Polynomial basis	
Operators		
$\dot{()}$	First time derivative	(()/s)
$\otimes$	Kronecker product	
$< \cdot >$	Inner product	
$\mathbb{E}[]$	Expectation	

Chapter 1

Introduction

1.1 Polynomial Chaos: State of the Art

Some key concepts within the field of stochastic computation will be introduced, alongside the necessary numerical methods. A fairly comprehensive review of historical development is provided, and particular emphasis is placed upon application to trajectory optimisation.

1.1.1 Uncertainty Quantification (UQ)

Accurate dynamic modelling is crucial to the vast majority, if not all, practical applications. From areas such as structural mechanics to trajectory design, numerical analysis plays a key role in design and development, and as such, precision is paramount. The objective when developing a simulation is to facilitate a deeper comprehension of the systems characteristics and thus, be able to predict any physical behaviours that may occur during operation. Extensive efforts have been devoted to the development of accurate numerical algorithms, in order to ensure that the generated predictions are reliable, and contain minimal numerical errors. It is only upon rigorous numerical analysis that a system is deemed suitable. Of course, in practice there are many factors that may arise, which could not have been accounted for previously. This can be due to measurement errors, or a lack of knowledge regarding the operating conditions - perhaps measurements are infrequent, or even unattainable. Therefore, it becomes obvious that appropriate treatment of these uncertainties must be integrated within the computational process, so that it becomes possible to fully understand the impact of errors, or uncertainty in parameter values, initial and boundary conditions.

Consequently, the field of Uncertainty Quantification (UQ) has become prominent in recent years, and as such, it has become conceivable to investigate the effect of such errors in measurements. As a result, more accurate and reliable predictions can be attained. Traditionally of primary interest to statisticians and risk modellers, the field has now branched into a wide variety of contexts. In particular, those which utilise complex systems, where mathematical models are a simplified, reduced order representation of the system in question. Although many models have been successful in revealing quantitative connections between predictions and observations, their usage is sometimes constrained by physical intuition[2]. Uncertainty encompasses the variability of data, and is unavoidable as a consequence of inaccurate or incomplete knowledge of the governing physics, lack of measurements, or indeed an error within them. Thus, if a full comprehension of the simulated behaviour, and later the real system, is to be achieved, this uncertainty must be incorporated throughout the numerical analysis - not merely as an afterthought.

Statistical risk analysis has long been the at the heart of the financial sector; for example, catastrophe models developed by insurance firms. Evidently, this process is hinged on the probabilistic nature of the event. Considering engineered systems continue to grow in complexity of operation and application, it also becomes essential that these deterministic models account for discrepancies in knowledge regarding their underlying physics or operational bounds. Introducing such an element of variability ensures the system is designed in a manner that fully incorporates this, and therefore helps build confidence in the system's integrity. Application of UQ techniques can be used for certification, prediction, model validation, parameter estimation, and inverse problems[2]. It can offer an invaluable insight into systematic and stochastic measurement error, limitations of theoretical models, and to some extent, human error.

1.1.2 Generalised Polynomial Chaos (gPC)

One of the most promising and widely used methods for UQ is Generalised Polynomial Chaos (gPC). Based on the original theory of Norbert Wiener in 1938, regarding Hermite Homogenous Chaos[3], it incorporates orthogonal polynomials to express the random quantities. Through exploitation of their inherent characteristics, the stochastic quantities are transformed into a set of augmented deterministic equations. The PC expansion will converge in the L_2 sense in the Hilbert space for stochastic systems with a finite second moment[4]. This generalisation was developed by Ghanem and Spanos and applied to many practical problems[5], as a framework to overcome some of the prior convergence issues when used in application to non-Gaussian problems. This is due to the fact that full convergence may only be achieved if the appropriate orthogonal polynomials are selected, based on the distributions of the random parameter[6]. This will be conveyed in more detail in the following Chapter, however, for now it is just necessary to understand the general procedure. The spectral representation in the random probability space demonstrates fast (and complete) convergence when the solution depends smoothly on the random parameters.

Upon selection of the appropriate polynomial basis, it is necessary to solve the problem using one of two methods. The first is the Galerkin method, which essentially minimises the error of the finite-order gPC expansion using projection principles. This results in a set of coupled deterministic equations that can then be solved using a numerical solver, such as Euler or Runge-Kutta. The second method is known as Stochastic Collocation, and this relies on repetitive calculations at each node within the random space. This is a deterministic sampling method and is based on the tensor products of nodes, through the use of Gauss quadrature[4]. A very important question is therefore presented - which method is best? Whilst the collocation principle offers relative ease of application, it is limited to low dimensionality. Errors can be introduced as a result of the integration scheme and aliasing effects. In comparison, Galerkin projection requires much fewer equations in order to achieve polynomial exactness. However, implementation is not as straightforward, as the Galerkin system must be derived. This can be an overwhelming process for complex, non-linear applications. For this reason, the Galerkin procedure is not as widely adopted, but it is of course a personal choice. For the purpose of this work, Galerkin is employed as it offers the most accurate solution for multi-dimensional problems, and does so using a minimal number of equations; thus, computational efficiency is ensured within some limits[7].

1.1.3 Applications of Stochastic Computation

Application of gPC theory to stochastic processes has become increasingly popular. The work of Wiener was the inspiration for the PC theory to follow, and focused on the decomposition of Gaussian stochastic processes; namely in regard to Brownian motion. However, it was Ghamen and Spanos who brought the topic into focus again. Their work within the field of Finite Element Analysis demonstrated the very practical benefits of PC application, although it was confined to Hermite polynomials of Gaussian random variables. This was later extended by Xiu and Karniadakis in 2002, when the proposal of the Generalised Polynomial Chaos (gPC) facilitated convergence for non-Gaussian problems[8]. This work detailed the selection process for the orthogonal polynomials based on the probability distribution function (PDF) of the random parameter. Xiu is now perhaps one of the most prominent researchers within the field and has released a number of papers on the application of gPC. Most recently, a textbook which has become a popular starting point for those who wish to utilise these methods. It offers a broad overview of numerical methods and fundamental concepts to gPC and the spectral approach. The applications of his work have largely been concerned with thermo-fluid behaviour[8][9]. Le Maıtre et al. extended the application of these techniques to fluid flow for low Mach number[10]. Debusschere et al. applied gPC to the context of electrochemical flow in micro-fluidic systems[11]. Most notably, the key figures within gPC research demonstrated the pitfalls and the challenges presented by its application[12]. Thus, highlighting the limitations of the method, and important considerations that must be made by anyone wishing to apply gPC in the context of their work.

1.1.4 Research within Robust Control

Evidently there are many benefits posed by application of PC methods, however, their application to controller design has only recently become apparent. Design of control algorithms that achieve robust performance in the presence of parametric uncertainty is certainly important. Development of gPC applications in the context of robust control became an interesting topic, most notably due to Nagy and Braatz, whom demonstrated the influence of parametric uncertainty upon non-linear systems in industrial applications such as batch crystallisation[13]. This served as a verification and validation technique, however, stability was not analysed. Application of gPC for stability analysis was first demonstrated by Hover and Triantafyllou, in which the stability of a simple bi-linear system was deduced from the gPC expansions. Hover later used a gradient based method to parametrise optimal trajectories using Legendre polynomials. This demonstrated that the method incurred low computational cost[14]. Considering that previously, incorporation of uncertainty within robust controllers was performed on a worst-case scenario basis. Consequently, the performance could in some cases be sluggish due to this over-compensation. It is for this reason that combination of robust control algorithms and stochastic control methods has become a very interesting development. By doing this, it becomes possible to first understand how random uncertainties impact upon the state trajectories of system in question. Secondly, it results in a less conservative controller design, thus ensuring the most effective performance. The stability margin of the controller is designed accounting for this parametric uncertainty, which results in a probabilistic robust control framework. It is also important to note that this optimisation process is also based on the distribution of parameters, and therefore the PDF must be known.

The techniques of gPC are valuable to the areas of non-linear filtering and parameter estimation, which rely on prediction of covariance. It has been demonstrated that it boasts better estimations for non-linear systems than those offered by linear propagation theory. In the work of Blanchard[15], the uncertainties are propagated and error covariances are estimated in the EKF framework. Parameter estimates are then obtained in the form of a polynomial chaos expansion, which possesses information about the a posteriori probability density function. Kewlani et al, presented further work regarding uncertainties in parameter estimation in application to autonomous vehicles[16]. The prediction of vehicle dynamics using gPC was proven to be more effective than Monte Carlo methods.

Monte Carlo (MC) is a sampling-based technique which generates independent realisations of the random parameters, which consequently become deterministic problems and random realisations of solutions are then obtained. It is a very popular method due its simplicity, and is usually the first method employed when analysing such problems. Unfortunately, the pure repetition required in order to obtain deterministic solutions places a very significant computational burden. The mean value generally converges at a rate inverse to the number of samples. Furthermore, it is not computationally scalable and can suffer statistical inconsistencies. MC is just one of the methods currently used in uncertainty propagation: Markov Chain MC, Bayesian Estimators and Unscented Kalman Filtering are some of the other methods used in non-linear estimation. The majority of gPC results are validated using one of these methods. High accuracy is demonstrated using gPC, with the added benefit of reduction in computational cost.

1.1.5 Application to Optimal Trajectory Design

It has been shown that gPC theory is reliable and effective when solving control problems with probabilistic uncertainty in system parameters. This work is specifically focused on the topic of optimal trajectory design and the mapping of the dynamic system to its higher order deterministic counterpart in consideration of structured uncertainties. The optimal control problem is essentially to determine the controls and states that optimise a performance cost, with respect to dynamic constraints. These are in the form of ordinary differential equations (ODEs), boundary conditions, and path constraints. The optimal cost, or Bolza problem, is solved using one of two classes of methods; direct or indirect. Indirect methods are based on Pontryagin's Principle, which states that the optimal cost function should result in the instantaneous minimisation of the Hamiltonian. However, this is reliant upon appropriate dual space variables[17]. This is achieved by formulation of the multiple-point boundary value problem (MPBVP), which results in high levels of accuracy. Unfortunately, it can be difficult to implement due to the need for initial costate guesses, which are not exactly intuitive. In consideration of this, direct methods are favourable and still gaining popularity due to their convenience and precision. They involve transcription of the Optimal Control Problem (OCP) into a finite dimensional, non-linear programming problem (NLP). SPARTAN[18;19;20;21;22;23] is a MATLAB tool developed at the German Aerospace Center (DLR), which utilises Pseudospectral (PS) techniques in order to solve the OCP. It will be used in this work to establish a framework for optimal trajectory calculation in consideration of stochastic uncertainties. If stochastic information is incorporated into the design and analysis phase, the trajectory can be amended accordingly in order to reduce strain on controllers; very important for practical applications. This is where uncertainty propagation again comes into focus, and in the same manner as the work detailed

previously, a more robust margin is obtained. For applications such as planetary landers and rovers, uncertainty is intrinsic. Whether it is manifested in the landing location, or as a consequence of mismatch in atmospheric conditions, failure to acknowledge this can be detrimental to the mission.

This work aims to build upon prior work carried out with regard to vehicle trajectory optimisation. The first to demonstrate this application was Prabhakar et al in 2010, where they presented a novel framework for analysis of uncertainty in hypersonic flight dynamics using gPC[24]. It concerned a Mars entry, descent and landing (EDL) problem, comprising of structured uncertainties in both the initial conditions and the state parameters. The evolution was then compared to MC results to verify the accuracy, and convey the computational efficiency of the method. Later that year, Dutta and Bhattacharya expanded this work by means of Bayesian estimations of the a priori probability density function of the random process, for the non-linear problem[25]. In consideration of the fact that Kalman filters are only optimal for linear systems, the Extended Kalman Filter must be applied to non-linear systems. In this method, the covariance is propagated from the current mean using the linear dynamics. Although, improvements in accuracy can be accomplished if propagation is performed using the non-linear dynamics. Thus, the density function is approximated and the posterior mean and covariance is determined to the third order. The combination of Bayesian estimator and gPC framework performed very well for the non-linear, hypersonic problem, in comparison to linear estimators. For instance, it was shown that EKF performs poorly for non-Gaussian parameter uncertainty.

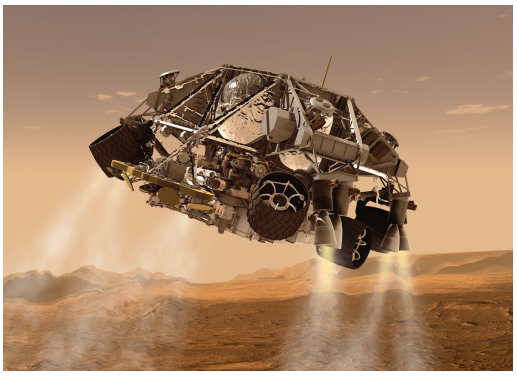

FIGURE 1.1: Mars Descent[1]

At this point it is important to specify the cost functionals that are presented within the gPC stochastic framework. Specifically, the aim is to deduce trajectories that result in minimum expectation and/or minimum variance. This was covered by Fisher and Bhattacharya in 2011, where they demonstrated that these were equivalent to the standard quadratic cost function[26]. Assuming the states are stochastic and the control input is deterministic. These principles were conveyed by means of the Van der Pol oscillator example, and results were compared to MC, as done in previous work. Most recently, the Van der Pol oscillator problem was also covered by Xiong et al[27]. Additionally, the hypersensitive problem was solved for two uncertainty sources. This particular problem is interesting, not only due to the multidimensional nature, but also the combination of both uniform and Gaussian distributions. Since a Polynomial Chaos Expansion (PCE) of $n = 2$ is deemed acceptable, efficient computational performance is ensured. When compared to a system with no stochastic elements incorporated, it becomes apparent that the resulting trajectory is less sensitive to the specified uncertainty and thus, more robust. A gliding

trajectory optimisation was also performed by Xiong, in addition to a comprehensive comparison of Intrusive and Non-Intrusive methods for PC (these definitions will later be formally defined)[28].

The elegant transformation from stochastic to deterministic problem offered by gPC methodology is evidently a very promising area of research. However, there are imposed limitations, which should not be overlooked or understated. In light of this, some of these crucial considerations are highlighted.

1.1.6 Numerical Challenges of gPC Methods

Previously, a distinction between Intrusive and Non-Intrusive PC methods was made. In the Intrusive case, the expansions are substituted into the governing equations and the evolution of uncertainty is obtained by Galerkin projection. This is conveyed by means of the spectral PCE coefficients. It is then transformed into the deterministic framework, however, subsequent arithmetic results in a number of issues. Most prominently, there are truncation errors in the Pseudospectral (PS) evaluation of polynomial basis functions and also in application to non-polynomial functions[12]. Additionally, it has been noted in the majority of the papers covered here, that an issue is presented in deviation of the PDF of the random variable from that of the associated PDF of the orthogonal polynomial. Not only does this degrade performance, it many also destabilise the governing equations. In a bid to combat this, high order PC representations must be used. As stated previously, usually a second order approximation is satisfactory, however, in the presence of high dimensionality i.e. many random variables, higher order approximations are necessary. More specifically, strictly positive variables that have small mean values and large uncertainties can pose severe challenges for the accuracy and stability of the PC representation. When large non-linearities are present, application of high PC order can be impractical, as the dimension of the problem grows very rapidly with order. Truncation errors also become more prevalent in such scenarios. PS methods offer a way in which to calculate high order problems in the most efficient and effective manner.

In application to non-polynomial functions, evaluations of PC variables are difficult, as the Galerkin projection method cannot be applied directly to determine the PC coefficients of the function result. Instead, another method used to overcome this is the Taylor series approximations for these functions. This was demonstrated by Debusschere et al[12]. Unfortunately, although straightforward and cost effective, yet again high-order PC expansions result in poor accuracy. Additionally, for many functions the limitation is set by the theoretical range of convergence of the Taylor series. A more robust and accurate technique was devised, which evaluates non-polynomial functions by integrating their derivatives. Furthermore, sampling-based methods can be employed; namely the non intrusive spectral projection method, which is capable of accurately evaluating functions of PC variables. Based on the degree of polynomial exactness of these quadrature rules, $M+1$ sample points in each stochastic dimension are sufficient to correctly integrate the expectations, if there is a well represented PC expansion of order M. Thus, accurate PC representations of functions may be obtained, but while efficient for a low M, the implementation results in dense tensor products in multiple dimensions. This then leads to an exponential increase in the number of samples, which of course degrades performance. It therefore becomes very apparent that these methods do not scale well with the number of stochastic dimensions in the problem. This is often referred to as "the curse of dimensionality" for dynamic programming.

Another crucial consideration is the response evolution. It was noted in the majority of research based on trajectory optimisation, that the accuracy is compromised the longer the integration time. Therefore, it can be stated that the gPC framework is well suited for evaluating short term statistics of dynamical systems, but is lacking in application to longer time periods. This occurs as a result of the finite dimensional approximation of the probability space. Prabhakar et al noted that lower order moments offer higher accuracy than higher order moments, for any given order of PCE[24].

In order to overcome these very significant limitations, computational and mathematical challenges have to be solved, and only following this will more general and practical applications evolve. In consideration of this so called "curse of dimensionality", more advanced sampling techniques would enable the efficient and accurate construction of a reduced basis space. A second requirement is to develop highly non-linear problems that expose reduced order methods for computational reduction. For this, there are several techniques which have been recently developed, such as: empirical interpolation and its discrete version. For example, best point interpolation, Gappy POD, Gauss Newton with approximated tensor[12]. However, these techniques do not necessarily guarantee the optimum formulation of the approximated problem. In particular its stability, which is necessary in order to enable reliable computational reduction. Furthermore, in the construction of reduced basis spaces, it is crucial to balance the errors arising from high-fidelity and reduced basis approximation, and this leads to a total error of the computational approximation of the underpinning parametric/stochastic problems. Depending on the problem, it is possible to be confronted with quantities whose variations with respect to the random parameters are not continuous. The gPC method experiences difficulties in convergence for such discontinuous distributions in the stochastic space. Additionally, it is important to note that the PDF cannot be determined explicitly in the gPC framework, unless a Gaussian distribution is adopted[29]. Other challenges, such as long-time integration behaviour, non-linear conservation laws and multi-scale and multi-physics coupling are also important for the development of reduced order methods; particularly for their application to uncertainty quantification problems[12].

1.1.7 Future Developments

The application of gPC can at first appear daunting; evidently it can become highly complex, and at an alarming rate. Additionally, the aforementioned issues can deter people from employing such techniques. Despite this, it is encouraging to see that there are a number of current research interests based on overcoming these challenges. Several methods have been proposed to reduce this divergence, including adaptive and multi-element approximation techniques. Dimension-adaptive sparse grid sampling, importance sampling, multi-level construction, are all in active development for reduced order methods in high-dimensional uncertainty quantification problems[12].

There has also been a peak in interest regarding high order stochastic collocation. The fundamental work regarding this principle was done by Xiu and Hesthaven, whom demonstrated an effective framework for this high order method[30]. The application of sparse grids for the purpose of multi-variate interpolation, results in high-order accuracy, with a reduced number of nodes in higher stochastic dimensions. It cannot be emphasised enough, just how challenging integration and interpolation become at this point. In an effort to reduce computational burden,

adaptivity is being explored; adaptive selection of polynomial basis, or adaptive sparse grid collocation.

Regarding the issue of discontinuous distributions in the stochastic space, it has been proposed that increasing the maximum degree of the chosen basis (p-refinement) helps. It must, however, be noted that despite some advantages, it cannot always overcome those convergence difficulties. It also expands the size of the system to solve, and hence makes the obtainment of the deterministic solution of the stochastic problem more complex. For longer integration times, convergence can be improved by a process referred to as time-dependent generalised polynomial chaos (TDgPC). This involves the recalculation of the polynomial basis after a specified time[31].

The regularity or, in some cases, irregularity of the solution with respect to the stochastic probability space has a significant effect on the convergence rate of gPC expansion. The difficulty is presented by the fact that this is usually not known a priori, for the majority of problems. This can be addressed by division of the stochastic space, in a method called "h-refinement". It facilitates use of a relatively low degree of expansion on each element of the partition, and this results in a piecewise polynomial approximation fitting. This is the basis of the multi-element generalised polynomial chaos (MEgPC). Wan and Karniadakis were the first to propose this decomposition of the random inputs into smaller elements. Consequently, in each element there is a new random variable that is produced, and then the standard gPC method can be applied. The methodology of this decomposition is based on a mesh adaptation scheme, which relies on the relative error in the variance prediction[32]. If an element does not satisfy the error criterion, the element is divided into two parts of equal dimensions. Further work has been proposed regarding the specified error criterion[31].

Finally, it is important to return to topic of optimal trajectory design specifically, and detail the proposed future work of the relevant researchers. In[24], they suggest future work will encompass the adaptive/multi-element techniques, as described previously in order to improve longer-term dynamics. Dutta and Prabhakar propose to generalise their Bayesian, gPC framework, in order to incorporate maximum likelihood and minimum error of the states and state estimates[24]. Finally, Xiong details the parallel computing technique for the transcription of the NLP as an area of interest. Additionally, more complex systems will be tackled[27].

The aim is ultimately, that through this fairly comprehensive review, the field of stochastic computations, and more specifically application of gPC theory becomes more transparent. The benefits of its application are evident and although some challenges are presented (particularly in the case of high dimensionality), the results are promising. By highlighting relevant research in the area of trajectory optimisation, it is hoped that this acts as a suitable benchmark for this work, and a solid foundation for extension of the methodology to a number of relevant problems. Successful application of gPC theory, along with the impressive ability of SPARTAN, will enable trajectory optimisation in the presence of structured uncertainty by development of a framework that solves for minimum covariance cost functionals. Most crucially, this will meet a key requirement in the design of future space missions.

Chapter 2

Mathematical Preliminaries

2.1 Definition of Problem Space

Some fundamental mathematical principles are discussed within this chapter in order to provide a foundation for the development of Polynomial Chaos methods.

2.1.1 Inner and Outer Products

The inner product is a more general form of the dot product that offers a way of multiplying vectors together within the defined vector space, resulting in a scalar. In a real vector space, the inner product is denoted by $\langle \cdot, \cdot \rangle$, where $(\cdot)$ corresponds to the appropriate variables[33].

Essentially, it is equivalent to the dot product between functions $f(\mathbf{x}), g(\mathbf{x})$, but in infinite dimensions and with different weightings. Orthogonality of the polynomials is intrinsically linked to the inner product, and thus it is a very important operation which will be detailed fully as follows.

The $\mathcal{L}_p$ space is also an important concept. The set of $\mathcal{L}_p$ functions must be p-integrable for f to be in $\mathcal{L}_p$ (i.e. $f(x_1, x_2, ..., x_p)$).

$$\|f\|_P = \left(\int_x \|f\|^p dx \right)^{1/p} \tag{2.1}$$

where x is the measure space.

The inner product space can also be referred to using $(\mathcal{L}_2, \langle \cdot, \cdot \rangle_2)$ and subsequently abbreviated by $\mathcal{L}_2$. This is the set of square integrable functions in the $\mathcal{L}^p$ space (in which $p = 2$). Therefore, it can be seen that $\mathcal{L}_p$ is a generalisation of $\mathcal{L}_2$.

The $\mathcal{L}_2$ norm, or the Euclidean norm as it is also known, is very simply the distance from the origin to point x, using Pythagorean theory.

The outer product is another important operation. It is the tensor product, which becomes particularly useful when building the polynomial bases:

$$f \otimes g = f(x)g(x)^T \tag{2.2}$$

The Kronecker product is a generalisation of the tensor product, and is also denoted by the symbol $\otimes$. For example, if A is an $[m \times n]$ matrix, and B is $[p \times q]$, then the Kronecker product is a matrix of dimension $[(mp) \times (nq)]$, defined as:

$$A \otimes B = \begin{bmatrix} a_{11}B & \dots & a_{1n}B \\ \vdots & \ddots & \vdots \\ a_{m1}B & \dots & a_{mn}B \end{bmatrix} \tag{2.3}$$

2.1.2 Hilbert Space

In order to define a Hilbert Space, it is necessary to start with some more basic definitions. First of all, a metric space, S, is a set in which the distance between two points, x and y, is a non-negative real number[34]. A distance function, d, in a metric space must satisfy the following conditions:

$$\begin{aligned} d(x,y) &= 0 \qquad \text{if} \quad x = y \\ d(x,y) &= d(y,x) \\ d(x,y) + d(y,z) &\geq d(x,z) \quad \text{triangle inequality} \end{aligned} \tag{2.4}$$

If the metric, or distance, d, satisfies the following limit, it is a Cauchy sequence, defined as:

$$\lim_{\min(m,n)\to\infty} d(x_m, y_n) = 0 \tag{2.5}$$

A complete metric space therefore results in every Cauchy sequence being convergent[35]. A Hilbert space, $\mathcal{H}$, is a vector space with an inner product $\langle f, g\rangle$ such that the norm, $\|f\|$

$$\|f\| = \sqrt{\langle f, f\rangle} \tag{2.6}$$

results in this complete metric space. The $\mathcal{L}_2$ is an example of an infinite-dimensional Hilbert space, $\mathcal{H}$, and in this case the inner product is given by[34]

$$\langle f, g\rangle = \int_{-\infty}^{\infty} w(x) f(x) g(x) dx \tag{2.7}$$

For $\mathcal{L}_p$ in which $p \neq 2$, the space is a Banach space, not a Hilbert space[36].

2.2 Orthogonal Polynomials

This section covers the main characteristics of orthogonal polynomials, and the classes that are particularly useful for this application.

2.2.1 Principle of Orthogonality

Orthogonal polynomials are a class, ψ_n, defined over the interval $[a, b]$ that obey the relation of orthogonality, which is defined as such[37]:

$$\int_a^b w(x)\psi_m(x)\psi_n(x)dx = \delta_{mn}\gamma_n \qquad m, n \in N \tag{2.8}$$

where $w(x)$ is a weighting function $(w(x) > 0)$ and δ_{mn} is the Kronecker delta, defined as:

$$\delta_{mn} = \begin{cases} 1, & m = n \\ 0, & m \neq n \end{cases} \tag{2.9}$$

The normalisation factor is denoted by γ_n and is the weighted inner product of the polynomials:

$$\gamma_n = \int_a^b w(x)[\psi_n(x)]^2 dx \tag{2.10}$$

If $\gamma_n = 1$ the polynomials are orthonormal and orthogonal, since an inner product of zero dictates the principle of orthogonality. Orthogonality is implied by the property of orthonormality, however, the opposite is not always the case; two vectors are orthonormal if they are orthogonal, and each vector has a norm of 1[37].

$$\langle u, v\rangle = 0 \quad \text{however} \quad \langle u, u\rangle = \langle v, v\rangle = 1 \tag{2.11}$$

The polynomials, ψ_n and ψ_m are defined in the standard manner[38].

$$\psi_n(x) = a_n x^n + a_{n-1}x^{n-1} + ... + a_1 x + a_0 \tag{2.12}$$

The monic version of $\psi_n(x)$ involves division by the leading coefficient, a_n. Orthogonality is a very useful property, which can help towards gaining the solution to a variety of mathematical and physical problems.

$$\psi_n(x) = x^n + \tilde{a_i}x^{n-1} + ... + \tilde{a_1}x + \tilde{a_0} \tag{2.13}$$

where,

$$\tilde{a_i} = \frac{a_i}{a_n}, \qquad i \in [0, ..., n-1] \tag{2.14}$$

There are various classes of polynomials which pose their own benefits of application. The most relevant to this work will now be discussed.

2.2.2 Three term Recurrence Relation for Orthogonal Polynomials

All sequences of orthogonal polynomials satisfy a three term recurrence relation given by[39]:

$$\psi_{n+1}(x) = (A_n x + B_n x)\psi_n(x) + C_n\psi_{n-1}(x) \quad n \in [1, ..., \infty] \tag{2.15}$$

where

$$A_n = \frac{a_{n+1}}{a_n} \quad n \in [0, ..., \infty] \quad \text{and} \quad C_n = -\frac{A_n}{A_{n-1}\cdot\frac{\gamma_n}{\gamma_{n-1}}} \quad n \in [1, ..., \infty] \tag{2.16}$$

Therefore, the sequence for a set of monic polynomials, i.e. for $a_n = 1$ is as follows:

$$\psi_{n+1}(x) = x\psi_n(x) + B_n\psi_n(x) + C_n\psi_{n-1}(x) \quad \text{with} \quad C_n = -\frac{\gamma_n}{\gamma_{n-1}} \tag{2.17}$$

This relationship provides a very powerful tool for generating the necessary polynomials, which will now be demonstrated.

2.2.3 Hermite Polynomials

Hermite polynomials, $H_n(x)$, are a set of orthogonal polynomials over an infinite domain $(-\infty, \infty)$. The weighting function is given by $e^{-x^2/2}$ for the Probabilists' class, whilst the Physicists' has a weighting of e^{-x^2}.

$$\int_{-\infty}^{\infty} H_m(x)H_n(x)e^{\frac{-x^2}{2}}dx = \delta_{m,n}n!\sqrt{2\pi} \tag{2.18}$$

The weight associated with this polynomial corresponds to a Gaussian distribution. The normalisation factor or inner product, denoted by $\langle H_n, H_n\rangle$, is given by $n!$.

As mentioned, there are two classes of Hermite polynomials; the Probabilists' is used here as the leading coefficient is 1, as opposed to 2^n for the former. The first few polynomials are as such:

$$\begin{aligned} H_0(x) &= 1 \\ H_1(x) &= x \\ H_2(x) &= x^2 - 1 \\ H_3(x) &= x^3 - 3x \\ &\vdots \end{aligned} \tag{2.19}$$

They satisfy the recurrence relationship of the form:

$$H_{n+1}(x) = xH_n(x) - H_{n-1}(x) \tag{2.20}$$

Using this relationship (Eq. (2.20)), the polynomials can be generated up to any order n and Fig. 2.1 depicts the Hermite polynomials up to $n = 3$.

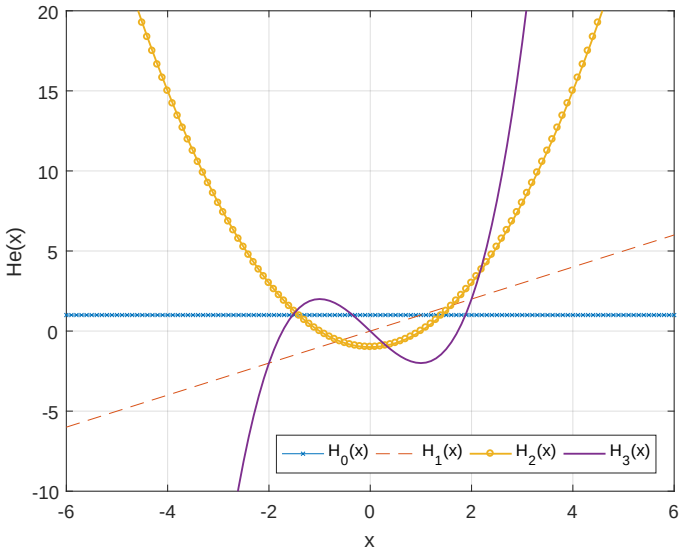

FIGURE 2.1: Probabilists' Hermite polynomials.

2.2.4 Legendre Polynomials

The second important class of polynomials are Legendre polynomials. These are related to a uniform distribution based on their weighting and are orthogonal with respect to the $\mathcal{L}_2$ norm on the interval $[-1 \leq x \leq 1]$.

$$\int_{-1}^{1} \psi_m(x)\psi_n(x)dx = \frac{1}{2n+1}\delta_{m,n} \tag{2.21}$$

Where $\delta_{m,n}$ is the Kronecker delta, as previously defined, and the preceding term is the normalisation, or inner product. The first few Legendre Polynomials are as follows:

$$\begin{aligned} L_0(x) &= 1 \\ L_1(x) &= x \\ L_2(x) &= \frac{1}{2}(3x^2 - 1) \\ L_3(x) &= \frac{1}{2}(5x^3 - 3x) \\ &\vdots \end{aligned} \tag{2.22}$$

They can be generated by means of Bonnet's recursion formula, and as before the polynomials of up to $n = 3$ are shown by Fig. 2.2:

$$(n+1)L_{n+1}(x) = (2n+1)xL_n(x) - nL_{n-1}(x) \tag{2.23}$$

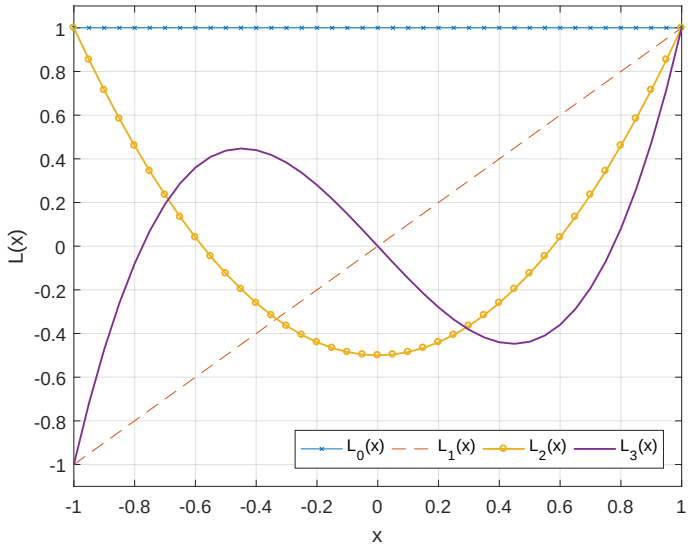

FIGURE 2.2: Legendre polynomials.

2.3 Gaussian Quadrature

In order to make quick, yet precise integral calculations quadrature techniques are utilised. This involves estimation of the function, $f(x)$, by a weighted sum for which the best approximation is achieved by selecting appropriate abscissas, $\mathbf{x_i}$. This is the case when the roots of the orthogonal polynomial, and the corresponding weighting function are used within the same interval. This domain of integration is $[-1, 1]$, and thus, the function must be well approximated by the polynomials within this range (i.e. not suited to those containing singularities). An n point Legendre-Gauss quadrature rule will be exact for all polynomials up to a degree of $2n - 1$.

$$\int_{-1}^{1} f(x)dx = \sum_{i=1}^{n} w_i f(x_i) \tag{2.24}$$

Since the abscissas, x_i, and the weights, w_i, are dependent on the specific polynomial, the following sections will detail how these are in fact obtained.

2.3.1 Hermite Quadrature

It is important to stress that the Probabilists' Hermite polynomials are used in this application, hence the calculated roots and weights must correspond to this. The first step in determining these quantities involves building the tri-diagonal Companion Matrix (CM), C, of the monic polynomial, $\psi(x)$, as given by Eq. (2.13).

$$C(a) = \begin{bmatrix} 0 & 1 & 0 & \dots & 0 \\ \vdots & \ddots & \ddots & \ddots & \vdots \\ \vdots & & \ddots & \ddots & \vdots \\ 0 & \dots & \dots & 0 & 1 \\ -a_n & \dots & \dots & \dots & -a_{n-1} \end{bmatrix} \in \mathcal{R}^{n\times n} \tag{2.25}$$

The CM can in fact be used to compute the zeroes of an n degree polynomial, as a consequence of this property:

$$\psi(x) = det[xI_n - C(a)] \tag{2.26}$$

It is therefore demonstrated by Eq. (2.26) that the roots of a given monic polynomial are equivalent to the eigenvalues, $\mathbf{D}$, of the CM. Furthermore, if $\psi(x)$ has distinct roots, the CM is diagonalisable. The eigenvectors, $\mathbf{V}$, are then calculated such that: $\mathbf{C} \times \mathbf{V} = \mathbf{V} \times \mathbf{D}$. This technique is known as the Jacobi method and is capable of finding the spectral decomposition of a symmetric matrix[40]. The weights, w_i, are simply the first column of the eigenvector matrix, V, squared.

The zeros and weights for Gaussian quadrature relating to the Probabilists' Hermite polynomials are given in Tab. 2.1 and Fig. 2.3 depicts the case of $n = 3$. Note that since this information is not as readily available as that for the physicists'[41;42], the results can be verified by comparing with the moments of a standard Gaussian variable[43].

TABLE 2.1: Hermite quadrature abscissas and weights up to $n = 5$

n	x_i	w_i
2	$\pm$ 1	0.5
3	$\pm$ 1.7321	0.1667
	0	0.6667
4	$\pm$ 2.3344	0.0459
	$\pm$ 0.7420	0.4541
5	$\pm$ 2.8570	0.0113
	$\pm$ 1.3556	0.2221
	0	0.5333

By ensuring full compatibility of the quadrature rule and the polynomials used, high precision can be achieved with very few nodes. For instance, with as little as 3 nodes, integrations are correct for a simple linear expression. Of course, as dimensionality increases, so does the number of nodes required to capture the behaviour.

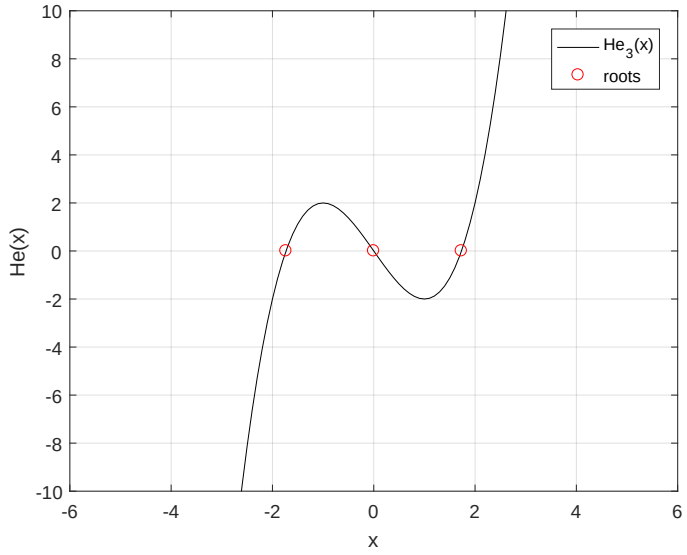

FIGURE 2.3: Roots of third order for probabilists' Hermite polynomial.

2.3.2 Legendre Quadrature

In order to calculate the roots of the Legendre polynomials, an initial guess is used; based on the roots of the Chebyshev polynomial's roots, which are given by:

$$x = cos\left(\frac{(2k+1)\pi}{2n}\right) \tag{2.27}$$

where k is the number of roots of the n degree polynomial. An iterative process is then performed using the Legendre recursion relationship until the zeroes are determined. The zeroes form the Legendre polynomial, $L(x_i)$, which has the derivative, $D(x_i)$. The corresponding weights, w_i are found as follows:

$$w_i = \frac{2}{(1 - {x_i}^2)D(x_i)^2} \tag{2.28}$$

The abscissas and weights are tabulated for up to $n = 5$ (Tab. 2.2), and the validity of the solution for $n = 3$ is demonstrated by Fig. 2.4.

TABLE 2.2: Legendre quadrature abscissas and weights up to $n = 5$

n	x_i	w_i
2	$\pm$ 0.5774	1
3	$\pm$ 0.7746	0.5556
	0	0.8889
4	$\pm$ 0.8611	0.3479
	$\pm$ 0.3400	0.6521
5	$\pm$ 0.9062	0.2369
	$\pm$ 0.5385	0.4786
	0	0.5689

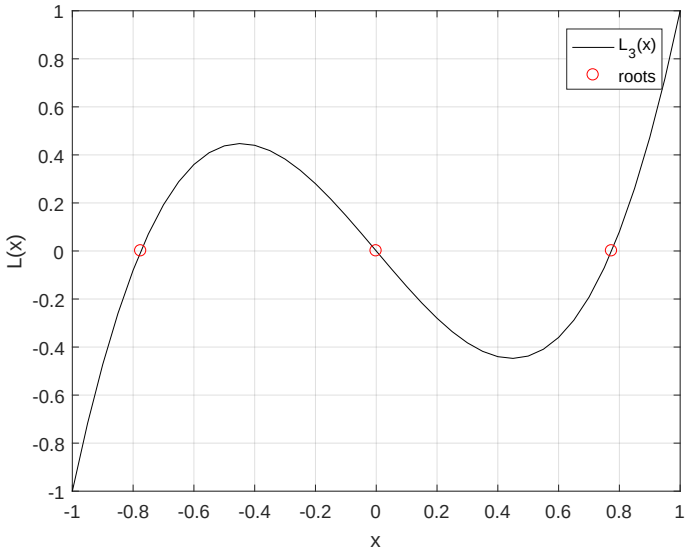

FIGURE 2.4: Roots of third order for Legendre polynomial.

2.4 Probability Theory

The likelihood of occurrence of an event is dictated by the concept of probability. The classic example is a coin flip; it is expected that the odds are $1:1$ for each face (50% likelihood of occurrence for each), if enough observations are made. Application of probability theory therefore provides a method for theoretical justification. The probability space is defined as a triplet $(\Omega, \mathcal{F}, P)$. The sample space is given by Ω, and this is the set of possible outcomes. For instance, using the coin analogy, the combinations of heads (H) and tails (T). The sample set is thus: HH, HT, TH and TT. The variation, σ, must ensure the collection of all events in the field, $\mathcal{F}$. The measurable space is therefore $(\Omega, \mathcal{F})$ and provides a means for determining the probability, P.

2.4.1 Gaussian Distribution

The Gaussian, or Normal distribution, is continuous and is defined as $\mathcal{N}(\mu, \sigma^2)$, where the mean, $\mu \in \mathbb{R}$ and the variance, $\sigma^2 \in \mathbb{R}$. The probability density function (PDF) is given by:

$$f(x) = \frac{1}{2\pi\sigma^2} e^{-\frac{(x-\mu)^2}{2\sigma^2}} \qquad x \in \mathbb{R} \tag{2.29}$$

The classic Normal distribution is defined with a mean, $\mu = 0$, and a standard deviation, $\sigma = 1$. This distribution (Figure 2.5) is compatible with the Hermite polynomials, as stated previously, due to their weighting. This means full convergence of the solution may be achieved.
A stochastic variable, **Z**, with mean, μ and standard deviation, σ, is therefore a function of the normally distributed variable **X** according to:

$$\mathbf{Z} = \mu + \sigma\mathbf{X} \tag{2.30}$$

where **X** has mean, $\mu = 0$, and standard deviation, $\sigma = 1$.

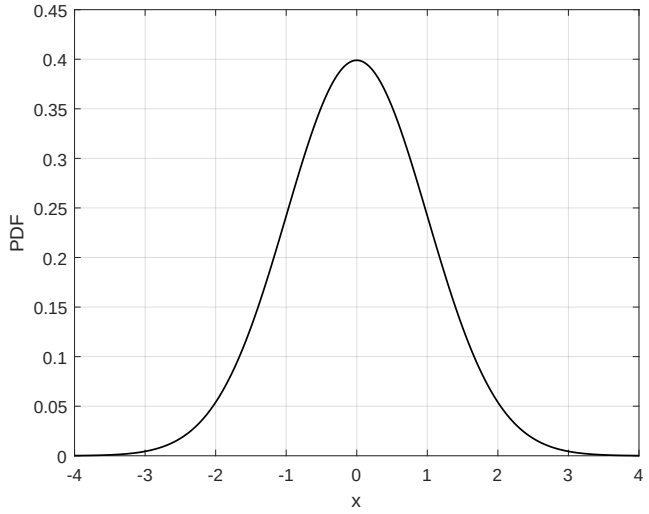

FIGURE 2.5: Gaussian distribution.

2.4.2 Uniform Distribution

The Uniform distribution is defined on the interval $U[a, b]$ and is given by the following density function:

$$f(\mathbf{x}) = \begin{cases} \frac{1}{b-a} & \mathbf{x} \in [a, b] \\ 0 & \text{otherwise} \end{cases} \tag{2.31}$$

Therefore, it can be seen that the distribution is a constant with respect to x. In order to be compatible with Legendre Polynomials, the distribution is $f(\mathbf{x}) = \frac{1}{2}$. This is due to the fact that the polynomials are defined in the interval $[-1, 1]$.

The mean, μ, and standard deviation, σ, can be defined using the specified upper and lower boundaries (b and a, respectively).

$$\mu = \frac{1}{2}(b + a) \tag{2.32}$$

$$\sigma = \frac{1}{12}(b - a)^2 \tag{2.33}$$

The probability distribution for the interval [-1,1], which corresponds to Legendre polynomials is depicted in Fig. 2.6:

In this case, the stochastic variable, **Z**, can be computed as:

$$\mathbf{Z} = a + (b - a)\mathbf{X} \tag{2.34}$$

where **X** is a uniformly distributed variable defined in $[0, 1]$ with mean, μ and standard deviation, σ.

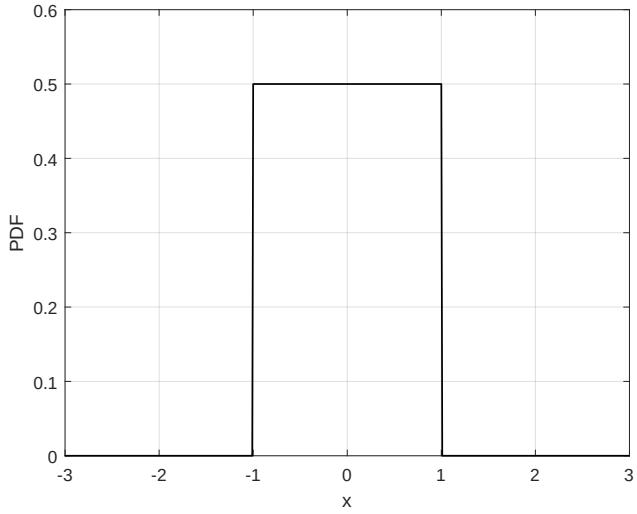

FIGURE 2.6: Uniform distribution.

2.4.3 Multi-dimensional Distributions

The distributions given previously correspond to a single random variable, however, for multivariate stochastic problems, the probability distribution function (PDF) must be amended appropriately. If the random variables are considered independent, that is to say that the occurrence of one does not impact that of the others, then the PDF is very simply the product of the univariate distributions.

$$f(x) = f_1(x)f_2(x)...f_n(x) \tag{2.35}$$

This means that the joint distribution is the product of the marginal density functions, which in this case is the same as the conditional distribution for each variable.

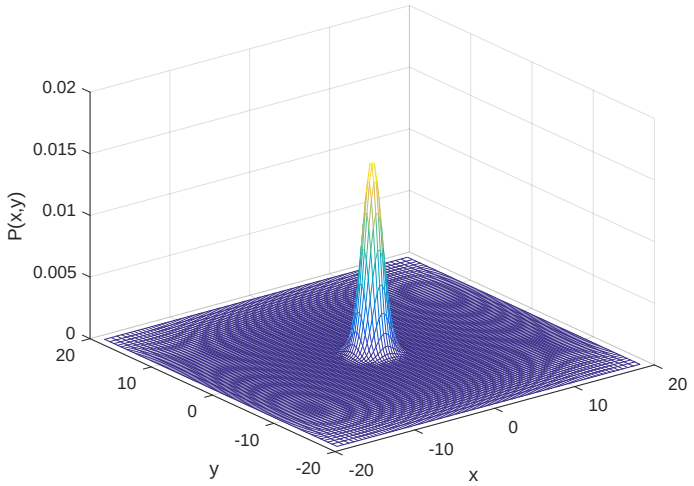

FIGURE 2.7: Joint normal PDF.

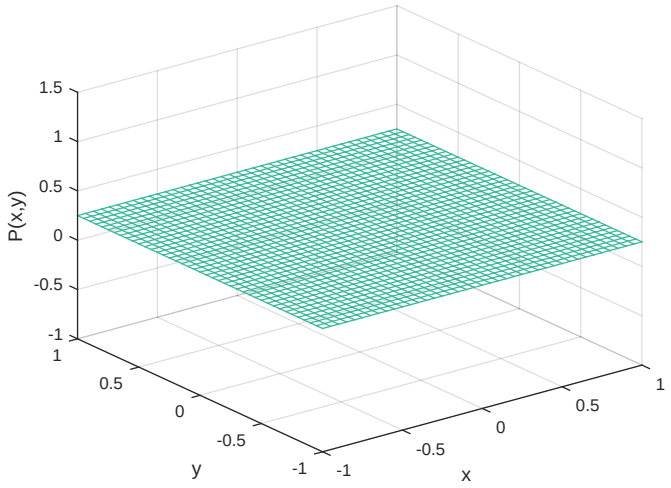

FIGURE 2.8: Joint uniform PDF.

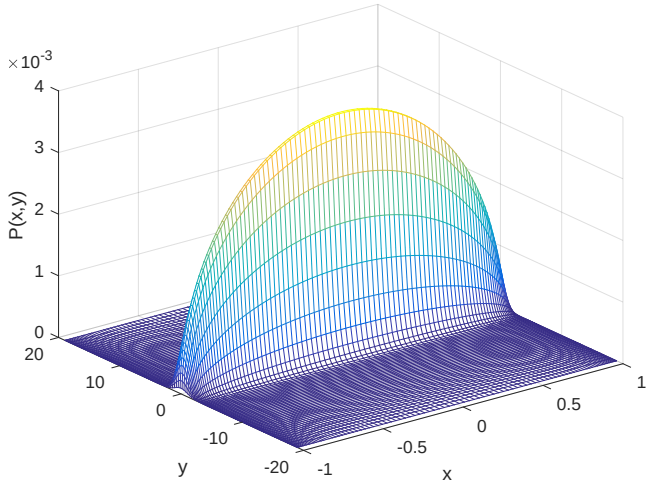

FIGURE 2.9: Joint mixed PDF.

2.4.4 Expectation and Moments

It is important to now define some key statistics within stochastic analysis. First of all, the mean value, also known as the expectation, is defined as:

$$\mu_X = \mathbb{E}[\mathbf{X}] = \int_{-\infty}^{\infty} x f(x) dx \tag{2.36}$$

where $\mathbf{X}$ is the random variable and the distribution is given by $f(x)$. In probability terms, it is deemed the most likely value to occur i.e. the peak of the PDF (see Fig. 2.5).

The variance, σ^2, is then a measure of the deviation from this mean, or most likely value, and is given by:

$$\sigma_X^2 = \mathbb{E}[\mathbf{X}] = \int_{-\infty}^{\infty} (x - \mu_X)^2 f(x) dx \tag{2.37}$$

The standard deviation, σ_X, is the square root of the variance and describes the spread of the variable around its mean, μ_X. In this way, it is usual that centred moments are considered, where the expectation is the centre and hence, the most likely value of the variable, $\mathbf{X}$. These are given by $\mathbb{E}[\mathbf{X} - \mu_X]^m$, where the m_{th} moment of $\mathbf{X}$ is given by:

$$\mathbb{E}[\mathbf{X}^m] = \int_{-\infty}^{\infty} x^m f(x) dx \qquad m \in \mathbb{N} \tag{2.38}$$

$$\sigma_X^2 = \mathbb{E}[\mathbf{X}^2] - \mu_X^2 \tag{2.39}$$

Simply, the first moment is the mean, μ_X, the second moment is the variance, σ_X^2, and the third is the skewness, γ. Higher moments become less intuitive, however, they are very rarely needed for this type of statistical analysis.

Having given an overview of some basic mathematical principles, it is now necessary to detail the formulation of the Polynomial Chaos Expansion (PCE) and exactly how these definitions are employed.

Chapter 3

Generalised Polynomial Chaos

3.1 Proposed Method for Stochastic Trajectory Optimisation

In this section the proposed stochastic trajectory optimisation method is described. First, the concept of polynomial chaos for uncertainty propagation is briefly summarised. Secondly, the Galerkin projection method to obtain the augmented system of differential equation is detailed. This projection leads to the proper definition of the underlying Augmented Optimal Control Problem (AOCP), which is ultimately solved with SPARTAN.

3.1.1 Uncertainty Propagation

In general terms, a dynamic system may be represented by means of Ordinary Differential Equations (ODEs) which can then be solved by a suitable numerical integration scheme (Runge Kutta, for instance). Let us consider a simple linear case,

$$\text{Deterministic dynamics} \quad \begin{cases} \dot{x}(t) = ax(t) \\ x(t_0) = x_0 \qquad\qquad t \in [t_0, t_f] \end{cases} \tag{3.1}$$

where $x \in \mathbb{R}$ is the state, and $a \in \mathbb{R}$ represents the system parameter. The initial state is denoted by x_0 and consequently integrated over the time span [t_0 t_f]. In the deterministic case (i.e., no uncertainties affect either x or a), this governing equation leads to a deterministic solution; however, in the presence of uncertainties Eq. (3.1) becomes a stochastic differential equation, which has a stochastic solution $x(t)$. A way to deal with stochastic systems is represented by the application of Polynomial Chaos Expansion (PCE). If we consider that stochastic quantities arise from both the parameters, a, and the initial conditions, x_0, then both the state $x(t)$ and the parameter a can be represented by the corresponding PCE models:

$$\text{PCE models} \quad \begin{cases} x(t) = \sum_{j=0}^{\infty} x_j(t)\psi_j(\xi) \\ a(t) = \sum_{i=0}^{\infty} a_i\psi_i(\xi) \end{cases} \tag{3.2}$$

The stochastic variables are represented by given by $\xi = [\xi_0, ..., \xi_d]$, where d is the number of uncertainties in the system. This infinite-dimensional expansion can be truncated at a suitable order, P, according to the work of Cameron and Martin, who stated full convergence in the $\mathcal{L}_2$ sense may be achieved upon appropriate orthogonal polynomial selection[44]. This truncation is performed in consideration of both numerical accuracy and computational cost. The correct choice is dependent on

TABLE 3.1: Orthogonal polynomial selection based on PDF of stochastic quantity

Distribution	Corresponding Polynomial	Interval	Weighting
Gaussian	Hermite	$(-\infty, \infty)$	$e^{-x^2/2}$
Uniform	Legendre	$[-1, 1]$	$\frac{1}{2}$

the weighting of the polynomial being compatible with the Probability Distribution Function (PDF), as highlighted in Table 3.1.

Consequently, the PCE models given by Eq. (3.2) are reduced to the P^{th} order approximation, and then substituted into the original ODE (Eq. (3.1)). Hence the stochastic linear system is

$$\sum_{k=0}^{P} \dot{x}_k(t)\psi_k(\xi) = \sum_{i=0}^{P}\sum_{j=0}^{P} a_i(t)x_j(t)\psi_i(\xi)\psi_j(\xi) \tag{3.3}$$

which represents a set of $P+1$ coupled differential equations. The extension to larger dimensions is obtained by applying the expansion to each of the terms involved in the original set of differential equations, and leads to the overall dimension of the problem, which is deduced using the following relationship,

$$P + 1 = \frac{(n+d)!}{n!d!} \tag{3.4}$$

where n is the highest order of polynomial used within the expansion, and the number of independent random variables is given by d. Further details on the multivariate expansion can be found in Appendix B. Therefore, $P + 1$ determines the number of PCE coefficients resulting from the expansion, which are used in order to transform the stochastic model into the corresponding deterministic augmented system. Unfortunately, the dimension of the problem will grow very rapidly with increasing n and/or d, thus creating significant computational burden. However, the curse of dimensionality is mitigated by

1. Choosing the set of basis functions corresponding to the uncertainty (for instance, for normally distributed variables an expansion of $n = 2$ is perfectly sufficient[4]).

2. Apply efficient multivariate integration techniques, based for instance on pseudospectral hyperquadrature rules.

3.1.2 Galerkin Projection

The next step is to perform the Galerkin projection, which will result in a set of $P+1$ deterministic equations. This coupled system is given by the following relationship, where $< \cdot >$ represents the inner product.

$$\dot{x}_k = \frac{1}{< \psi_k^2(\xi) >} < \sum_{j=0}^{P} x_j(t)\psi_j(\xi), \sum_{i=0}^{P} a_i(t)\psi_i(\xi), \psi_k(\xi) > \quad k \in [0, ..., P] \tag{3.5}$$

The inner product of the orthogonal polynomials is the integral of the product of univariate or multivariate polynomial bases, $\psi_k(\xi)$, and the probability distribution, $F(\xi)$.

$$< \psi_i(\xi), \psi_j(\xi) > \quad = \int_a^b \psi_i(\xi)\psi_j(\xi)F(\xi)d\xi \tag{3.6}$$

where the limits a and b are the integral bounds for the respective distribution (see Table 3.1). Note that in the multivariate case, the PDF is then simply the product of the marginal distributions for each random variable, if they are mutually independent. Thus, even in the case of mixed distribution problems, the system characteristics can be captured well.

The initial PCE coefficients are given by a_i, which consist of the mean, μ and standard deviation, σ of the parameter, a. For one dimensional problems, these properties of the random parameter are placed in the first and second entries respectively, of the matrix of dimension $[1 \times P]$ (i.e. $a_i = [\mu_a, \sigma_a, 0, ..., 0]$). However, in the multi-dimensional case it is slightly different (which will be described fully as follows). If we now denote the integral of the triple product given by Eq. (3.6), as e_{ijk}, and the normalization factor (as it is also known), as γ_k, then the augmented system can be written in such a manner:

$$\dot{x_k} = \frac{1}{\gamma_k} \sum_{i=0}^{P} \sum_{j=0}^{P} a_i x_j e_{ijk} \tag{3.7}$$

where,

$$e_{ijk} = \mathbb{E}[\psi_i(\xi)\psi_j(\xi)\psi_k(\xi)] \tag{3.8}$$

and

$$k \in [0, 1, ..., P], \quad \gamma_k = \quad < \psi_k(\xi), \psi_k(\xi) > \tag{3.9}$$

Note that for the one dimensional case, there exists an analytical solution[37] for the integral of the triple product, e_{ijk}, and the normalization factor, γ_k, for Hermite and Legendre polynomials, i.e., Gaussian and Uniformly distributed random quantities, ξ. Specifically, we have:

Hermite polynomials:

$$e_{ijk} = \begin{cases} \frac{i!j!k!}{(s-i)!(s-j)!(s-k)!}, & \gamma_k = k! \quad \text{if Eq. (3.12) holds} \\ 0 \quad \text{otherwise} \end{cases} \tag{3.10}$$

Legendre polynomials:

$$e_{ijk} = \begin{cases} \left((-1)^s \sqrt{\frac{(2s-2i)!(2s-2j)!(2s-2k)!}{(2s+1)!}} \frac{s!}{((s-i)!(s-j)!(s-k)!}\right)^2, & \gamma_k = \frac{1}{2k+1} \quad \text{if Eq. (3.12)} \\ 0 \quad \text{otherwise} \end{cases} \tag{3.11}$$

The orthogonality conditions are given by:

$$s \geq i, j, k \quad \text{and} \quad 2s = i + j + k \quad \text{is even} \tag{3.12}$$

The solutions can of course also be obtained using the quadrature methods. If only one uncertainty is introduced, then the order of these polynomials is simply given by the indices i, j and k. However, in the multivariate case, the polynomial bases

are built using a Graded Lexicographic indexing method[4 45]. This indexing method involves generating an array of indices of dimension $[(P+1) \times d]$ and essentially involves generating every combination of integers whose sum equals the order of polynomial expansion, n. For example, consider a problem with 2 uncertain quantities ($d = 2$), and with a third order PCE ($n = 3$). Using this method, the polynomial bases are built as follows, where the subscript following ψ denotes the order of polynomial and the subscript following ξ corresponds to the appropriate random variable (Table 3.2).
The integral of the triple product, e_{ijk}, for the multivariate case is therefore found using cubature techniques (i.e., quadrature for higher dimensions).

TABLE 3.2: Multi-Index Method for $\mathbf{n = 3}$, $\mathbf{d = 2}$.

$\|i\|$	α	Single index k	Polynomial basis
0	0 0	1	$\psi_0(\xi_1)\ \psi_0(\xi_2)$
1	1 0	2	$\psi_1(\xi_1)\ \psi_0(\xi_2)$
	0 1	3	$\psi_0(\xi_1)\ \psi_1(\xi_2)$
2	2 0	4	$\psi_2(\xi_1)\ \psi_0(\xi_2)$
	1 1	5	$\psi_1(\xi_1)\ \psi_1(\xi_2)$
	0 2	6	$\psi_0(\xi_1)\ \psi_2(\xi_2)$
3	3 0	7	$\psi_3(\xi_1)\ \psi_0(\xi_2)$
	2 1	8	$\psi_2(\xi_1)\ \psi_1(\xi_2)$
	1 2	9	$\psi_1(\xi_1)\ \psi_2(\xi_2)$
	0 3	10	$\psi_0(\xi_1)\ \psi_3(\xi_2)$

Now the integral, e_{ijk}, is also generated using the relation given by Eq. (3.8), however, the single integer is now of dimension d, corresponding to the number of independent stochastic variables. The polynomial bases function to be evaluated in the tensor product of the product of univariate polynomials in each dimension. For example, if we consider a two-dimensional problem, then the polynomial basis function is generated as such:

$$\Psi_1 = \psi_i(\xi_1)\psi_j(\xi_1)\psi_k(\xi_1)w \quad \Psi_2 = \psi_i(\xi_2)\psi_j(\xi_2)\psi_k(\xi_2)w \quad i,j,k \in [0,...,P-1] \tag{3.13}$$

where, w, is the weight associated with the respective uncertainty. The Kronecker tensor product is then taken and the resultant basis function, Ψ, is integrated using cubature techniques.

$$\Psi = \Psi_1 \otimes \Psi_2 \tag{3.14}$$

The integers i, j, k are the original single indices but now they dictate which row of the multi-index is used. Within this row, the first column corresponds to the first uncertainty. *Note that if there is initial condition uncertainty on any of the states, it will be placed first within the multi-index.* A generalised representation this PCE can be viewed in Appendix A. For clarity, the first few terms of the expansion are depicted by Fig. 3.1. Here you can see that i increments in this nested loop structure.

When building the polynomial basis for the PCE, it is important to make two clear distinctions - the case of non-linearity in the dynamics and non-linearity arising from the uncertainties. This is especially important when you begin to consider MIMO systems. As the state, x, increases in dimension, the number of univariate

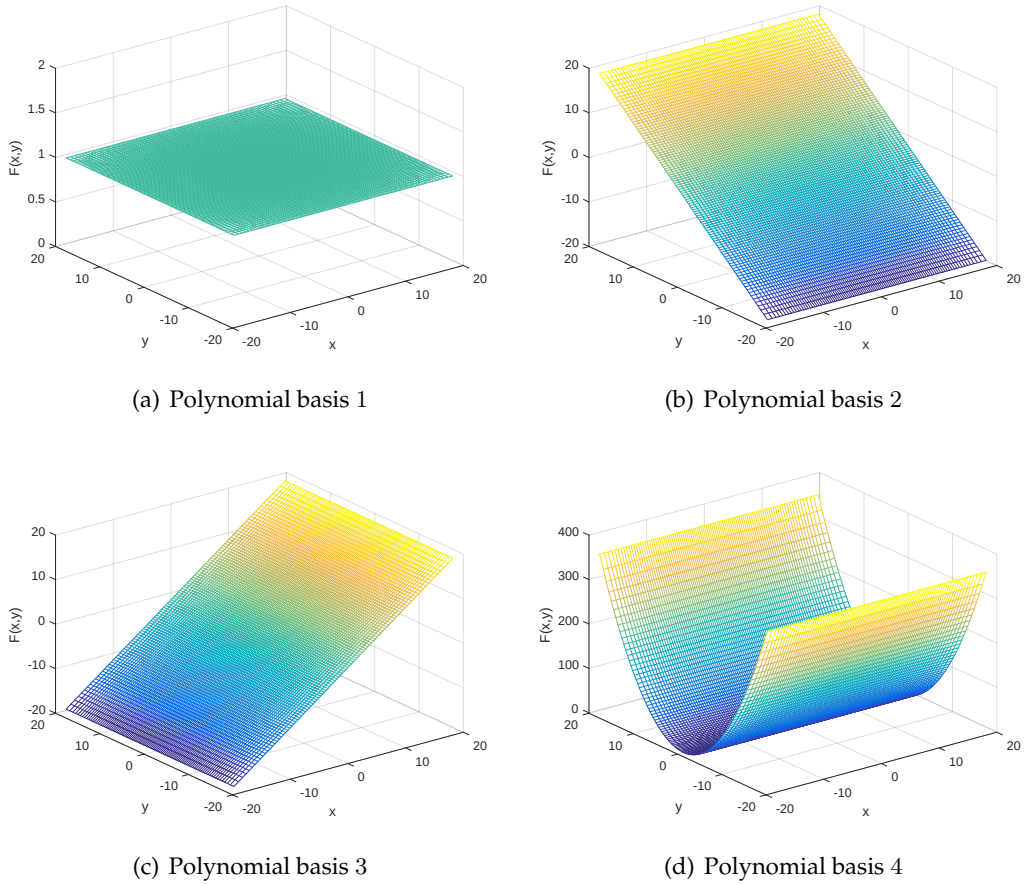

(a) Polynomial basis 1

(b) Polynomial basis 2

(c) Polynomial basis 3

(d) Polynomial basis 4

FIGURE 3.1: Hermite polynomial bases for $2d$ uncertainty: (a) $i = 0$ $j = 0$ $k = 0$ (b) $i = 1$ $j = 0$ $k = 0$ (c) $i = 2$ $j = 0$ $k = 0$ (d) $i = 3$ $j = 0$ $k = 0$

polynomials, ψ, in each basis function, Ψ, increases. However, as the number of uncertainties within the system as a whole increases, the number of bases increase too i.e. it is the Kronecker product of d bases. This will be made more obvious in the numerical examples covered in Ch. 5.

The multi-index, α, is also intrinsically linked to the initial PCE coefficients, a_i, and dictates the positioning of the distribution parameters (μ_a and σ_a). Taking the example given for $n = 3, d = 2$, the initial PCE coefficients are thus given by $\mathbf{a_i} = [\mu_a, 0, \sigma_a, 0, ..., 0]$. The corresponding polynomial bases will define a tensor product (also called Kronecker product, denoted by $\otimes$) given in the fourth column of Table 3.2. The normalization factor, γ_k, will be defined accordingly as the product of the univariate γ_k:

Hermite polynomials:

$$\gamma_k = \prod_{i=0}^{d} \alpha_i! \tag{3.15}$$

Legendre polynomials:

$$\gamma_k = \prod_{i=0}^{d} \frac{1}{2\alpha_i + 1} \tag{3.16}$$

Remark 3 Two classes of Hermite polynomials exist: physicists' and probabilists'. Here the latter is used. In the case of Legendre polynomials, there are also two variations: normal and shifted. They each have different normalization factors and thus, care must be taken to ensure full compatibility

In the case of mixed distributions, the normalization is simply the product of the respective normalization factors, γ_k. By solving these integrals it is possible to compute an augmented matrix, A, that is used in the system of equations. For example, let us consider the linear case as before, but now with a control input, u subject to the parameter, b (i.e., a continuous-time linear system):

$$\text{LTI system} \quad \begin{cases} \dot{x}(t) = ax(t) + bu(t) \\ x(0) = x_0 \end{cases} \tag{3.17}$$

We then assume that there is uncertainty in the variable x (i.e., resulting from parameter, a, and/or initial condition, x_0), whilst the control, u is deterministic (b is constant). The stochastic system representing Eq. (3.17) is given by the augmented linear system

$$\dot{\mathbf{x}}(t) = A\mathbf{x}(t) + B\mathbf{u}(t) \tag{3.18}$$

where the transformation matrix A will be of dimension $[(P+1) \times (P+1)]$ and is computed such that

$$A_{jk} = \frac{1}{\gamma_k} \sum_{i=0}^{P} \sum_{j=0}^{P} a_i e_{ijk} \quad k \in [0, ..., P] \tag{3.19}$$

Since we assumed a deterministic control parameter, the corresponding transformation matrix is simply B = $[1, 0, ..., 0]^T$ and is also of length $P + 1$.

The system of Eq. (3.19) can be propagated in order to obtain the PCE coefficients (as now given by each of the components of $\mathbf{x}$). The initial values of $\mathbf{x}$ are defined by $\mathbf{x}_0$, which correspond to the first PCE coefficients of the initial condition. For instance, if there is uncertainty in the initial conditions, then $\mathbf{x_0} = [\mu_x, \sigma_x, 0, ..., 0]$. If uncertainty is only in the parameter, a, then $\mathbf{x}_0$ will only consist of μ_x as a non-zero term. Now the generation of the multivariate PCE has been discussed, it is now necessary to detail how this is used to the transform the OCP in order to account for the system uncertainties.

Chapter 4

Definition of Stochastic Optimal Control Problem

4.1 Augmented Optimal Control Problem

In order to obtain the optimal control, $\mathbf{u}^*$, for a stochastic system, the cost function must be modified in order to account for the uncertainties in the system. This is achieved by using the derived deterministic dynamics resulting from the PCE and subsequent Galerkin projection. Consequently, the augmented system will be described by the $P+1$ states, obtained by the PCE expansion. Since we are dealing with stochastic systems, we do not minimise deterministic variables, but stochastic quantities, such as the mean, and the standard deviation. This information needs to be properly incorporated into the cost function as well. In the frame of PCE, the mean and the standard deviation are defined as

$$\begin{aligned} \mu &= x_0(t) \\ \sigma &= \sqrt{\sum_{i=1}^{P} \gamma_i {x_i}^2(t)} \end{aligned} \tag{4.1}$$

By this definition, the mean always corresponds to the first PCE coefficient, $\mathbf{x_0}$, whilst the standard deviation is the sum of the product of normalisation factor and corresponding PCE coefficient (neglecting the mean, x_0).

We can therefore define the AOCP as follows:

$$\underbrace{AOCP}_{determine\ u^*} = \begin{cases} \min \quad J = \Phi[\mu(\mathbf{x}), \sigma(\mathbf{x})] + \displaystyle\int_{t_0}^{t_f} \Psi[\mu(\mathbf{x}), \sigma(\mathbf{x})] dt \\ s.t. \quad \dot{x}_k = \dfrac{1}{< \psi_k^2(\xi) >} < \displaystyle\sum_{i=0}^{P} \sum_{j=0}^{P} a_i(t) x_j(t) \psi_i(\xi) \psi_j(\xi), \psi_k(\xi) > \\ \quad \mathbf{x_0}(t_0) = x_0(t_0), ..., x_p(t_0) \\ \quad \mathbf{x_f}(t_f) = x_0(t_f), ..., x_p(t_f), \quad k \in [0, ..., P]. \end{cases}$$

The cost is comprised of the Mayer and Lagrange terms, as previously defined, hence the first term imposes final state conditions, whilst the former regulates the entire response. The specific stochastic cost formulation depends on both the original cost and the desired restrictions on mean and/or variance.

For instance, if we wish to minimise the expectation of the square of the final state,

then this can be written in terms of the PCE in the following manner[26]:

$$\mathbb{E}[x^2] = \sum_{i=0}^{P}\sum_{j=0}^{P} x_i x_j \int \psi_i(\xi)\psi_j(\xi)d\xi = \mathbf{X}(t)^T W \mathbf{X}(t) \tag{4.2}$$

$$W = diag[< \psi_0(\xi), \psi_0(\xi) >, ..., < \psi_k(\xi), \psi_k(\xi) >] \tag{4.3}$$

where W denotes the weights corresponding to the inner products (which are also given by γ_k) and $\mathbf{X}$ contains the PCE coefficients.

If we now consider minimum covariance trajectories, then the variance, $\sigma^2(x)$ can also be written in terms of the PCE expansion as:

$$\sigma^2(x) = \mathbb{E}[x - \mathbb{E}[x]]^2 = \mathbb{E}[x^2] - \mathbb{E}^2[x] = \mathbf{X}(t)^T W \mathbf{X}(t) - \mathbb{E}^2[x] \tag{4.4}$$

where,

$$\begin{aligned} \mathbb{E}[x] &= \mathbf{X}(t)^T F \quad \text{and} \quad F = [1, 0, ..., 0]^T \\ \mathbb{E}^2[x] &= \mathbf{X}(t)^T F F^T \mathbf{X}(t) \end{aligned} \tag{4.5}$$

This can therefore be further simplified:

$$\sigma^2(x) = \mathbf{X}(t)^T (W - FF^T)\mathbf{X}(t) \tag{4.6}$$

This formulation results in the attainment of optimal control solutions for minimum expectation and/or covariance trajectories following the PCE and subsequent Galerkin projection. The relations given by Eqs. (4.5) and (4.6) can enter the cost in integral form or as a final condition.

The process of stochastic trajectory optimisation is now outlined, and now these principles are demonstrated using two case problems in order to convey exactly how the deterministic augmented system is obtained.

4.1.1 Overview of Stochastic Trajectory Optimisation Procedure

The proposed framework for stochastic trajectory optimisation can be summarised by the following steps which are also depicted in Fig 4.1:

1. Model uncertainties within the system using PCE.
2. Transform stochastic system of equations into the augmented deterministic equivalent.
3. Quantify the stochastic cost functional (dependent of whether minimum expectation and/or covariance trajectory).
4. Solve augmented system by NLP transcription (using SPARTAN, in this case) in order to establish the optimal control.
5. Calculate the relevant statistics for the new optimised trajectory.

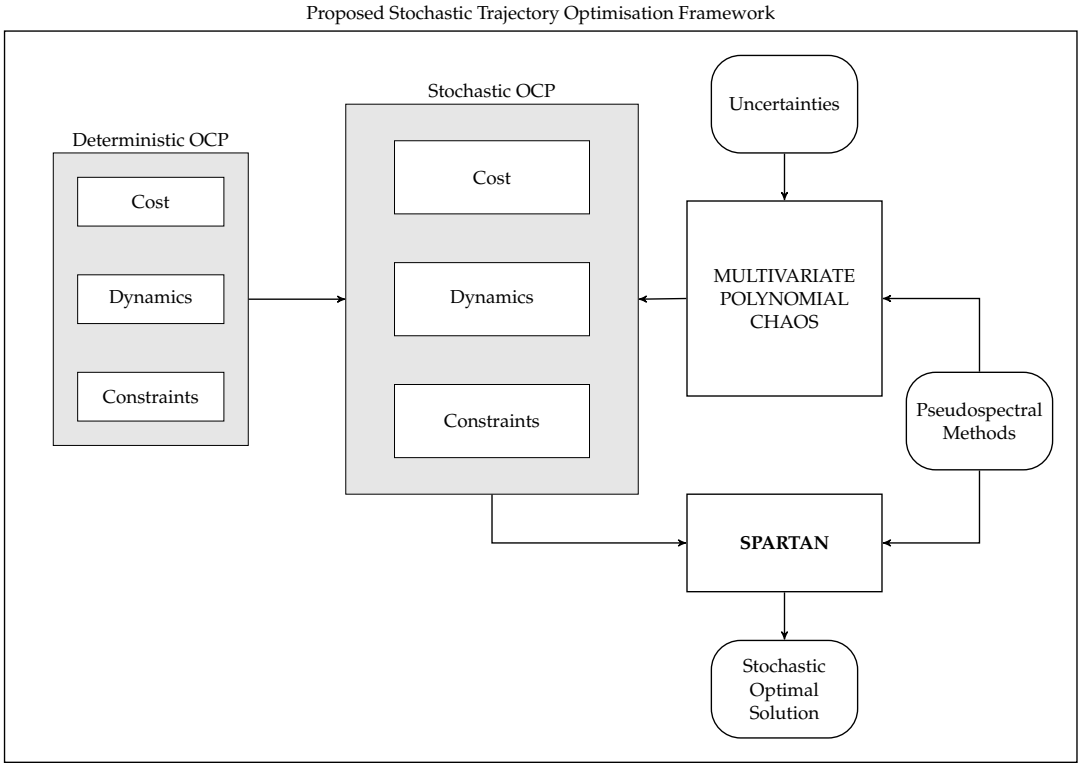

FIGURE 4.1: Overview of stochastic trajectory optimisation using multivariate polynomial chaos.

Chapter 5

Numerical Examples

A number of examples are given in order to demonstrate the capability of Multivariate Polynomial Chaos in application to stochastic trajectory optimisation. First of all, the one-dimensional case is given and this is subsequently extended to multi-dimensional uncertainty. The results presented as follows were obtained for minimum final expectation and variance of the stochastic trajectory.

5.1 Example Zero

This chapter details the example that was used during the development of the Polynomial Chaos techniques. It does not involve any optimisation process, but is beneficial to include for the purposes of demonstrating the validity of the method and solution. This can be achieved as there exists a number of analytical solutions for the uncertainties, which can be further verified using a very simple MC. Furthermore, the example has been covered by others[27] and thus, it is possible to directly compare results to check that the augmented system is indeed correct.

The following system is a linear example subject to a parameter, a:

$$\begin{aligned} \dot{x}(t) &= -ax(t) \\ x(0) &= 1, \quad t = [0,1]s \end{aligned} \tag{5.1}$$

If we first consider an uncertainty in the initial condition of $x_0 \sim N(1, 0.2)$ and a deterministic parameter, a, then the PC model is as given by Eq. (3.2). The initial PCE coefficients for the parameter, a, will therefore be $\mathbf{a_i} = [1, 0, 0]$, and those for the initial condition will be $\mathbf{x_0} = [1, 0.2, 0]^T$. Since there is no uncertainty in the parameter, the augmented system obtained from Eq. (3.19) is simply:

$$\dot{\mathbf{x}} = \begin{bmatrix} \dot{x}_0 \\ \dot{x}_1 \\ \dot{x}_2 \end{bmatrix} = - \begin{bmatrix} 1 & 0 & 0 \\ 0 & 1 & 0 \\ 0 & 0 & 1 \end{bmatrix} \mathbf{x}, \qquad \gamma = \begin{bmatrix} 1 \\ 1 \\ 2 \end{bmatrix} \tag{5.2}$$

The analytical expressions in this case for the mean, $\overline{\mu}$, and standard deviation, $\overline{\sigma}$, are given by:

$$\begin{aligned} \overline{\mu} &= \mu_x(e^{-at}) \\ \overline{\sigma} &= \mu_x(e^{-a_0 t})\sigma_x \end{aligned} \tag{5.3}$$

Finally, a Monte Carlo (MC) analysis of 2000 runs is performed by simply perturbing the initial condition by δx, where:

$$\delta x = \mu_x + \sigma_x Z \tag{5.4}$$

where μ_x is the mean of the initial condition, σ_x, is the initial state standard deviation and $\mathbf{Z}$ is a vector of normally distributed random numbers of dimension $[n \times 1]$. Here n is the number of MC runs.

The augmented system of equations is propagated in order to determine the system statistics as shown in Figs. 5.1(a) and 5.1(b). These statistics have been obtained using the PCE coefficients and Eqs. (4.5) and (4.6) and are compared to the MC value and the analytical one. All three solutions demonstrate full agreement.

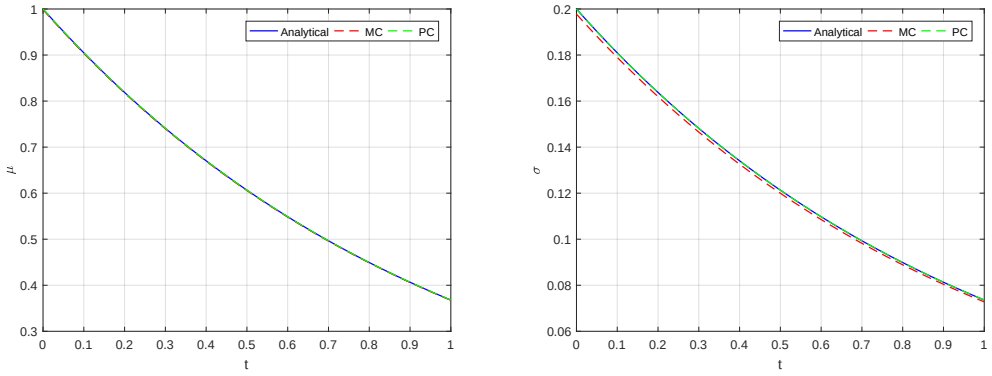

(a) Mean for $1d$ normal initial condition.

(b) Std for $1d$ normal initial condition.

FIGURE 5.1: Statistics for $1d$ normal initial condition (a) mean, and (b) std.

The coefficients resulting from propagation of the augmented system are given by Fig. 5.12. There are only 3 since the number of random variables, $d = 1$, and the order of expansion $n = 2$, according to Eq. (3.4).

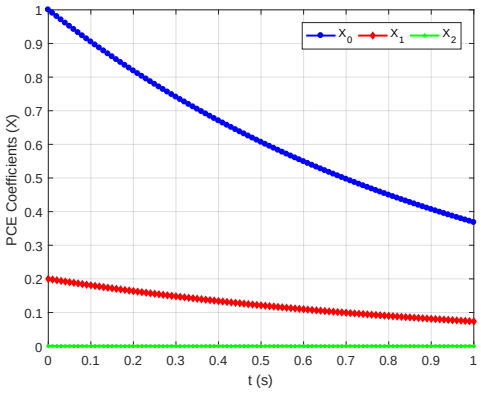

FIGURE 5.2: PCE coefficients for normal initial condition uncertainty.

Now moving on to parameter uncertainty of $a \sim N(0, 1)$, then the initial coefficients are $\mathbf{a_i} = [0, 1, 0]$ and $\mathbf{x}_0 = [1, 0, 0]^T$. This is due to the fact that the mean, μ, is assigned to the first coefficient, and for $1d$ uncertainty the second coefficient is σ. The augmented system is given by:

$$\begin{bmatrix} \dot{x}_0 \\ \dot{x}_1 \\ \dot{x}_2 \end{bmatrix} = - \begin{bmatrix} 0 & 1 & 0 \\ 1 & 0 & 2 \\ 0 & 1 & 0 \end{bmatrix} \begin{bmatrix} x_0 \\ x_1 \\ x_2 \end{bmatrix}, \qquad \gamma = \begin{bmatrix} 1 \\ 1 \\ 2 \end{bmatrix} \tag{5.5}$$

The analytical solutions for mean, $\overline{\mu}$ and standard deviation, $\overline{\sigma}$, for $1d$ normal parameter uncertainty are as follows:

$$\begin{aligned} \overline{\mu} &= e^{(\frac{1}{2}(\sigma_a t)^2 - \mu_a t)} \\ \overline{\sigma} &= \sqrt{e^{2(\sigma_a t)^2 - 2\mu_a t} - e^{(\sigma_a t)^2 - 2\mu_a t}} \end{aligned} \tag{5.6}$$

A comparison between the analytical, MC and PC statistic solutions are presented in Figs. 5.3(a) and 5.3(b). The PCE coefficients are shown depicted in Fig. 5.12. Evidently, a second order approximation is not sufficient to capture the standard deviation for high uncertainties. Instead, a PCE of $n = 4$ can demonstrate the evolution of the stochastic quantity perfectly. This particular example is covered in Ch. 6 for reference.

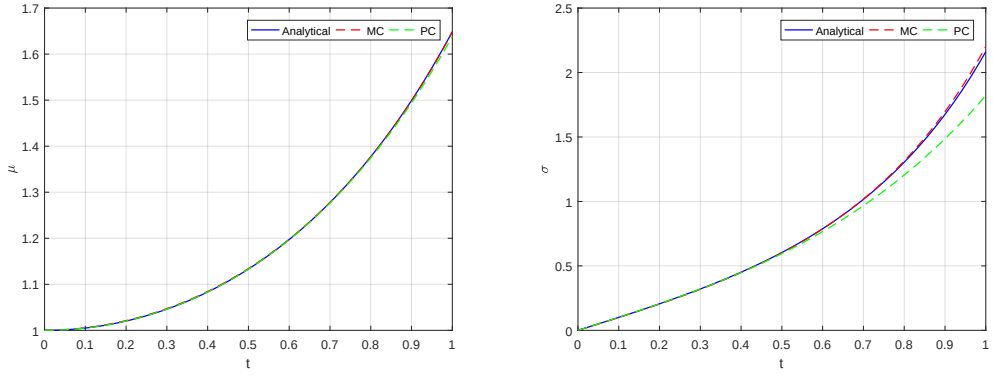

(a) Mean for $1d$ normal parameter.

(b) Std for $1d$ normal parameter.

FIGURE 5.3: Statistics for $1d$ normal parameter (a) mean, and (b) std.

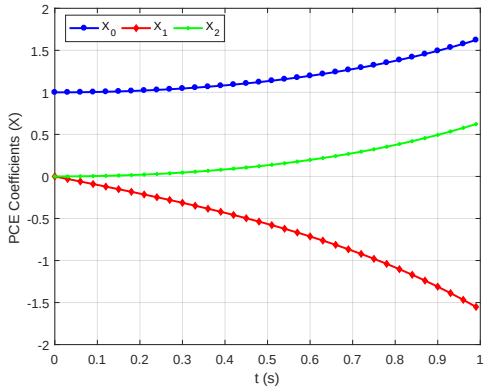

FIGURE 5.4: PCE coefficients for $1d$ normal parameter.

For uniform parameter uncertainty $a \sim N(-1, 1)$, the initial PCE coefficients are $\mathbf{a_i} = [0, 1, 0]^T$ and $\mathbf{x_0} = [1, 0, 0]^T$. The subsequent augmented system is given by:

$$\dot{\mathbf{x}} = \begin{bmatrix} \dot{x}_0 \\ \dot{x}_1 \\ \dot{x}_2 \end{bmatrix} = - \begin{bmatrix} 0 & 0.3333 & 0 \\ 1 & 0 & 0.4 \\ 0 & 0.6667 & 0 \end{bmatrix} \begin{bmatrix} x_0 \\ x_1 \\ x_2 \end{bmatrix}, \qquad \gamma = \begin{bmatrix} 1 \\ 0.3333 \\ 0.2 \end{bmatrix} \tag{5.7}$$

The analytical solutions are as follows, where the upper boundary is denoted by u_b and the lower by l_b. The subscript a corresponds to the parameter:

$$\begin{aligned} \overline{\mu} &= -\frac{e^{-u_{ba}t} - e^{-l_{ba}t}}{t(u_{ba} - l_{ba})} \\ \overline{\sigma} &= \sqrt{-\frac{e^{-2u_{ba}t} - e^{-2l_{ba}t}}{2t(u_{ba} - l_{ba})} - \overline{\mu}^2} \end{aligned} \tag{5.8}$$

As before, the statistics are compared in Figs. 5.5(a) and 5.5(b), and it is apparent that uniform distributions can be captured more precisely than normal distributions when using lower polynomial orders. There are 3 coefficients shown in Fig. 5.12.

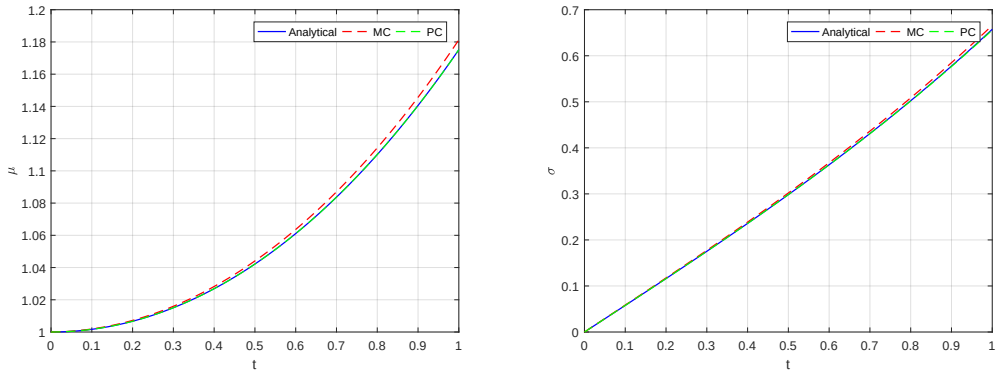

(a) Mean for $1d$ normal parameter.

(b) Std for $1d$ normal parameter.

FIGURE 5.5: Statistics for $1d$ uniform parameter (a) mean, and (b) std.

Next, we start to consider the two-dimensional case where the is uncertainty in both

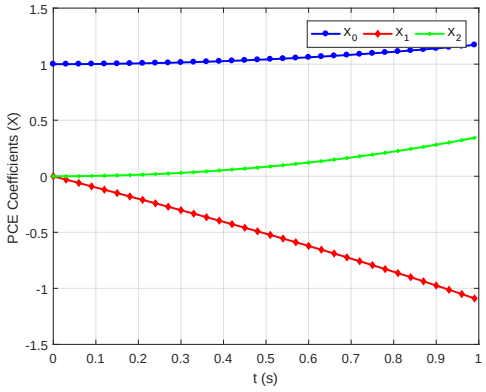

FIGURE 5.6: PCE coefficients for $1d$ uniform parameter.

the parameter and initial condition. For example, if $a \sim N(0, 1)$, with initial condition uncertainty of $x_0 \sim N(1, 0.2)$ and an expansion of $n = 2$, the initial PCE coefficients are $\mathbf{a_i} = [0, 0, 1, 0, 0, 0]^T$ and $\mathbf{x_0} = [1, 0.2, 0, 0, 0, 0]^T$. It is important to pay attention to the placement of the standard deviation term, which corresponds to the placement of the first non-zero in the multi-index (n.b. initial conditions are always placed

first). The augmented system is then as such:

$$\begin{bmatrix} \dot{x}_0 \\ \dot{x}_1 \\ \dot{x}_2 \\ \dot{x}_3 \\ \dot{x}_4 \\ \dot{x}_5 \end{bmatrix} = - \begin{bmatrix} 0 & 0 & 1 & 0 & 0 & 0 \\ 0 & 0 & 0 & 0 & 1 & 0 \\ 1 & 0 & 0 & 0 & 0 & 2 \\ 0 & 0 & 0 & 0 & 0 & 0 \\ 0 & 1 & 0 & 0 & 0 & 0 \\ 0 & 0 & 1 & 0 & 0 & 0 \end{bmatrix} \begin{bmatrix} x_0 \\ x_1 \\ x_2 \\ x_3 \\ x_4 \\ x_5 \end{bmatrix}, \qquad \gamma = \begin{bmatrix} 1 \\ 1 \\ 1 \\ 2 \\ 1 \\ 2 \end{bmatrix} \tag{5.9}$$

The analytical solution for the $2d$ normal problem is:

$$\begin{aligned} \overline{\mu} &= \mu_x e^{\frac{1}{2}(\sigma_a t)^2 - \mu_a t)} \\ \overline{\sigma} &= \sqrt{(\sigma_x^2 + \mu_x^2) e^{2\sigma_a^2 t^2 - 2\mu_a t} - \mu_x^2 e^{\sigma_a^2 t^2 - 2\mu_a t} - \mu_x^2 e^{\sigma_a^2 t^2 - 2\mu_a t}} \end{aligned} \tag{5.10}$$

The expectation comparison is given in Fig. 5.9(a), whilst the standard deviation is depicted in Fig. 5.9(b). These statistics are derived from the 6 PCE coefficients which are shown in Fig. 5.8.

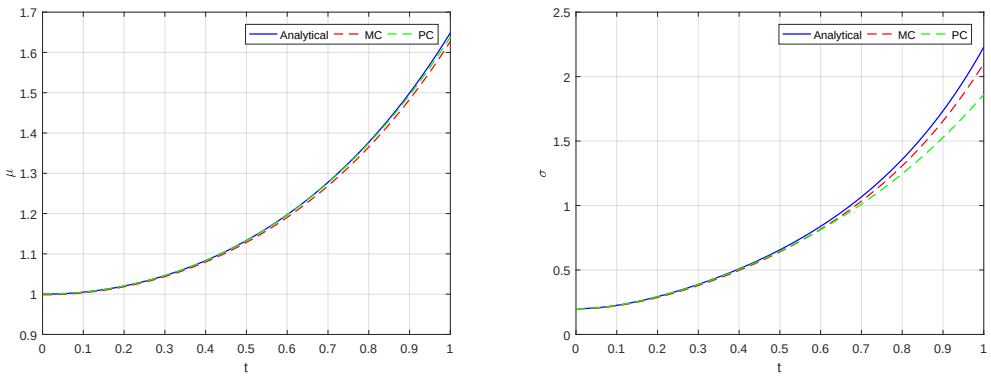

(a) Mean for $2d$ normal parameter and initial condition.

(b) Std for $2d$ normal parameter and initial condition.

FIGURE 5.7: Statistics for $2d$ normal parameter and initial condition (a) mean, and (b) std.

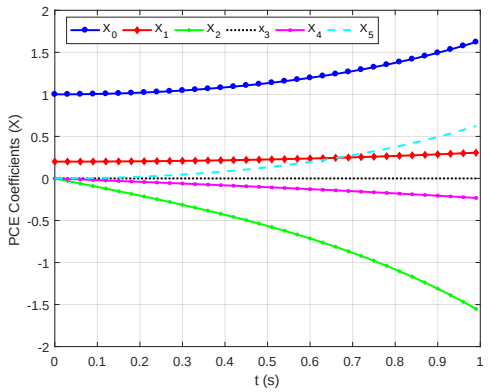

FIGURE 5.8: PCE coefficients for $2d$ normal parameter and initial condition uncertainty.

For $2d$ uniform distribution of $a \sim U(-1, 1)$, with initial condition uncertainty of $x_0 \sim U(0.4, 1.6)$ the initial conditions are $\mathbf{a_i} = [0, 0, 1, 0, 0, 0]^T$ and $\mathbf{x_0} = [1, 0.6, 0, 0, 0, 0]^T$ and the augmented stochastic system is therefore.

$$\begin{bmatrix} \dot{x}_0 \\ \dot{x}_1 \\ \dot{x}_2 \\ \dot{x}_3 \\ \dot{x}_4 \\ \dot{x}_5 \end{bmatrix} = - \begin{bmatrix} 0 & 0 & 0.3333 & 0 & 0 & 0 \\ 0 & 0 & 0 & 0 & 0.3333 & 0 \\ 1 & 0 & 0 & 0 & 0 & 0.4 \\ 0 & 0 & 0 & 0 & 0 & 0 \\ 0 & 1 & 0 & 0 & 0 & 0 \\ 0 & 0 & 0.6667 & 0 & 0 & 0 \end{bmatrix} \begin{bmatrix} x_0 \\ x_1 \\ x_2 \\ x_3 \\ x_4 \\ x_5 \end{bmatrix}, \qquad \gamma = \begin{bmatrix} 1 \\ 0.3333 \\ 0.3333 \\ 0.2 \\ 0.1111 \\ 0.2 \end{bmatrix} \tag{5.11}$$

The analytical expression for $2d$ uniform uncertainty in both the parameter and initial condition:

$$\begin{aligned} \overline{\mu} &= \frac{1}{2}(u_{bx} + l_{bx}) - \frac{e^{-u_{ba}t} - e^{-l_{ba}t}}{t(u_{ba} - l_{ba})} \\ \overline{\sigma} &= \sqrt{-\frac{1}{3}(u_{bx}^2 + l_{bx}^2 + l_{bx}u_{bx})\frac{e^{-2u_{ba}t} - e^{-2l_{ba}t}}{2t(u_{ba} - l_{ba})} - \overline{\mu}^2} \end{aligned} \tag{5.12}$$

For the $2d$ case, 5000 MC runs were performed in order to establish to reach agreement with the gPC solution and the analytical value. Again, uniform uncertainty is well captured by using the PC framework, even for a small expansion of $n = 2$. The statistics are shown by Figs. 5.9(a) and 5.9(b). The PC coefficients are depicted in Fig. 5.10.

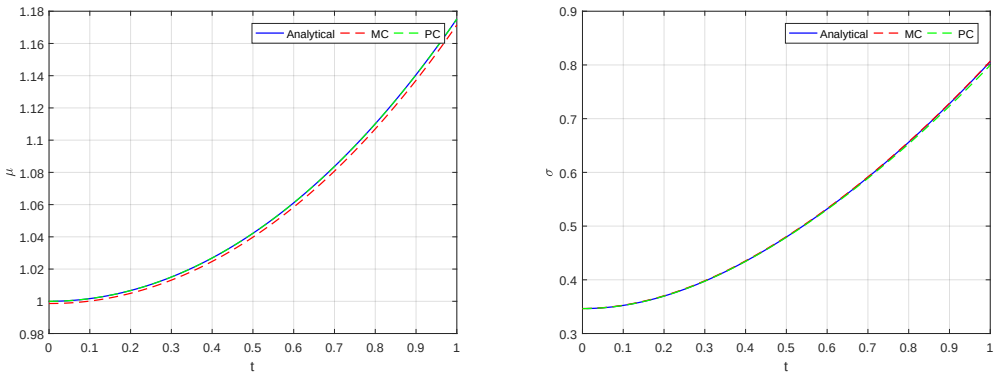

(a) Mean for $2d$ uniform parameter and initial condition.

(b) Std for $2d$ uniform parameter and initial condition.

FIGURE 5.9: Statistics for $2d$ uniform parameter and initial condition (a) mean, and (b) std.

Finally, if we consider the mixed distribution case: a normal parameter uncertainty

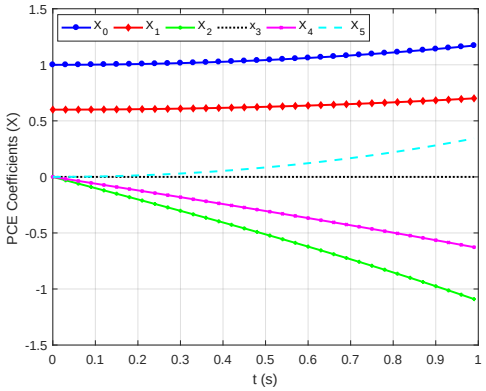

FIGURE 5.10: PCE coefficients for $2d$ uniform parameter and initial condition uncertainty.

$a \sim N(0,1)$, with initial condition uncertainty of $x_0 \sim U(0.4, 1.6)$, then the initial conditions are $\mathbf{a_i} = [0,0,1,0,0,0]^T$ and $\mathbf{x_0} = [1, 0.6, 0, 0, 0, 0]^T$.

$$\begin{bmatrix} \dot{x}_0 \\ \dot{x}_1 \\ \dot{x}_2 \\ \dot{x}_3 \\ \dot{x}_4 \\ \dot{x}_5 \end{bmatrix} = - \begin{bmatrix} 0 & 0 & 1 & 0 & 0 & 0 \\ 0 & 0 & 0 & 0 & 1 & 0 \\ 1 & 0 & 0 & 0 & 0 & 2 \\ 0 & 0 & 0 & 0 & 0 & 0 \\ 0 & 1 & 0 & 0 & 0 & 0 \\ 0 & 0 & 1 & 0 & 0 & 0 \end{bmatrix} \begin{bmatrix} x_0 \\ x_1 \\ x_2 \\ x_3 \\ x_4 \\ x_5 \end{bmatrix}, \qquad \gamma = \begin{bmatrix} 1 \\ 0.3333 \\ 1 \\ 0.2 \\ 0.3333 \\ 2 \end{bmatrix} \tag{5.13}$$

Again we define the analytical expression for verification purposes:

$$\begin{aligned} \overline{\mu} &= \frac{1}{2}(u_{bx} + l_{bx}) e^{\frac{1}{2}\sigma_a^2 t^2 - \mu_a t} \\ \overline{\sigma} &= \sqrt{-\frac{1}{3}(u_{bx}^2 + l_{bx}^2 + l_{bx} u_{bx}) e^{\sigma_a^2 t^2 - \mu_a t}} \end{aligned} \tag{5.14}$$

The resultant statistics are given by 5.11(a) and 5.11(b).

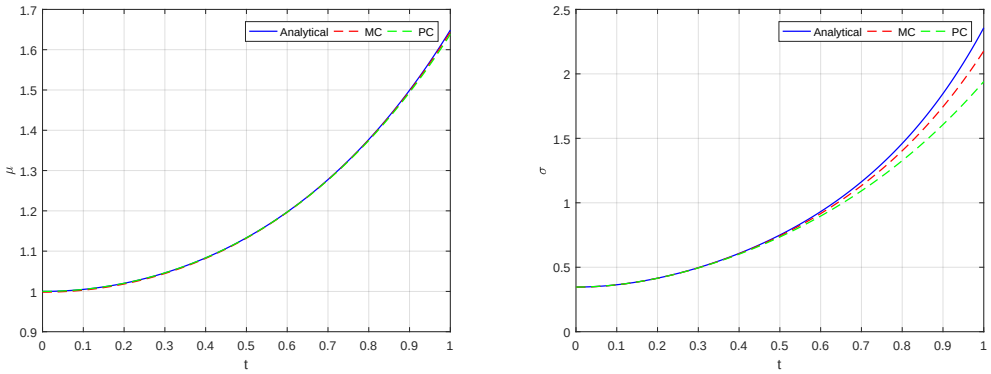

(a) Mean for $2d$ normal parameter and uniform initial condition.

(b) Std for $2d$ normal parameter and uniform initial condition.

FIGURE 5.11: Statistics for $2d$ normal parameter and uniform initial condition (a) mean, and (b) std.

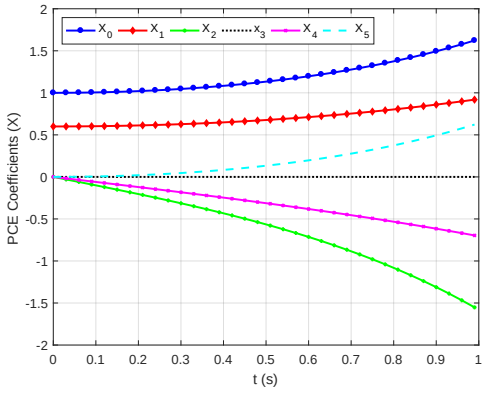

FIGURE 5.12: PCE coefficients for $2d$ normal parameter and uniform initial condition uncertainty.

These examples have demonstrated the basic structure of the PC framework and how uncertainty is propagated within the system. The difference in application to univariate and multivariate problems has been made clear and it is now possible to move onto increasingly complex examples. More specifically, the following examples will encompass the optimisation process and exactly how the gPC framework benefits stochastic trajectory design.

5.2 Linear Example

The first numerical example is an LTI system (as given by Eq. (3.17)). The problem is to minimise the norm of final state, $x(t_f)$, subject to time and control constraints. The optimisation problem is formulated as such:

$$\begin{aligned} \min \quad & J = x^2(t_f) \\ & \dot{x}(t) = ax(t) + bu(t) \\ s.t. \quad & \|u(t)\| \leq 10 \\ & x(0) = 2, \quad t = [0, 5]s \end{aligned} \tag{5.15}$$

where $a = 1$ and $b = 1$ in the deterministic case. In order to determine exactly how uncertainty impacts upon the trajectory, both parameter uncertainty and initial condition uncertainty are explored. The distribution for the parameter is normal, $a \sim N(1, 0.05)$. The initial condition uncertainty also has a normal distribution, $x_0 \sim N(2, 0.001)$.

First of all, one-dimensional parameter uncertainty is demonstrated in order to highlight the differences in implementation between that and the multi-dimensional problem. If $a \sim N(1, 0.05)$, then for a second order expansion $(n = 2)$ there will be $n + 1$ coefficients, and the initial parameter PCE coefficients are $\mathbf{a_i} = [1, 0.05, 0]$. Considering there is no uncertainty in the initial conditions (ie., $\sigma_x = 0$), the initial condition PCE coefficients are $\mathbf{x_0} = [1, 0, 0]^T$. The transformation matrix, A, as given by Eq. (3.19), is determined and the augmented system of equations is then:

Remark 4 Note that PCE values have been further validated using the PCET toolbox[46], in order to verify the method and accuracy of quadrature techniques.

$$\dot{\mathbf{x}} = \begin{bmatrix} \dot{x}_0 \\ \dot{x}_1 \\ \dot{x}_2 \end{bmatrix} = \begin{bmatrix} 1 & 0.05 & 0 \\ 0.05 & 1 & 0.1 \\ 0 & 0.05 & 1 \end{bmatrix} \begin{bmatrix} x_0 \\ x_1 \\ x_2 \end{bmatrix} + \begin{bmatrix} 1 \\ 0 \\ 0 \end{bmatrix} u \tag{5.16}$$

This system is then solved by SPARTAN and the new optimal control solution is obtained for the stochastic trajectory. The AOCP now involves minimizing the square of expectation and standard deviation (i.e., variance). Now, in order to establish whether the new control profile is in fact more robust in the presence of this uncertainty, a Monte Carlo (MC) analysis is performed. Both the original deterministic and the new stochastic systems are perturbed and the mean, μ, and standard deviation, σ, are calculated. The effect on the control profile can be seen in Fig. 5.13(a), whilst the corresponding PCE coefficients are shown in Fig. 5.13(b). Finally, the MC analysis consisting of 1000 runs is demonstrated by Fig. 5.14, where it is very apparent that the newly obtained stochastic control is far less perturbed by the uncertainty in parameter. Considering this linear system is inherently unstable, it is rather impressive that the expectation converges to a minimum value of 0.07528 using the new stochastic control, in comparison to 2.4589 in the deterministic case. It is apparent that the original control solution offers no robustness to the uncertainty; exhibiting wide divergence (with an std of 11.8551).

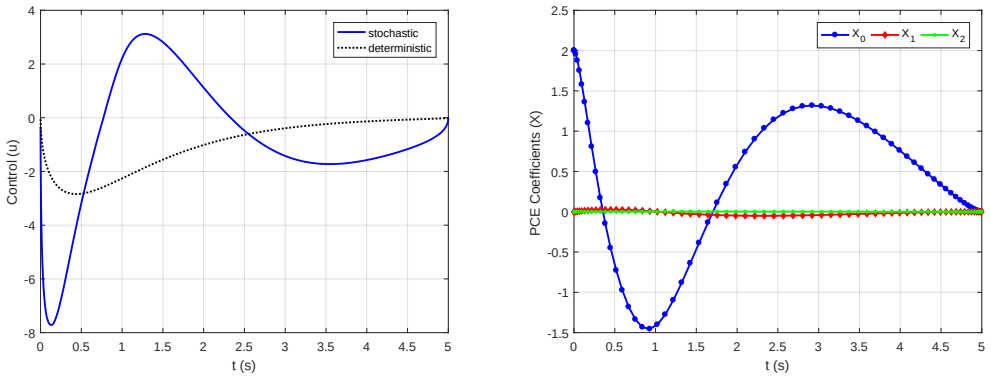

(a) Control for 1d linear problem.

(b) PCE coefficients for 1d problem.

FIGURE 5.13: 1d uncertainty: (a) 1d control comparison, and (b) 1d PCE coefficients.

Now if both parameter and initial condition uncertainty are considered, the initial parameter PCE coefficients are $\mathbf{a_i} = [1, 0, 0.05, 0, 0, 0]$ and $\mathbf{x_0} = [2, 0.001, 0, 0, 0, 0]^T$. The augmented system to be solved is therefore:

$$\dot{\mathbf{x}} = \begin{bmatrix} \dot{x}_0 \\ \dot{x}_1 \\ \dot{x}_2 \\ \dot{x}_3 \\ \dot{x}_4 \\ \dot{x}_5 \end{bmatrix} = \begin{bmatrix} 1 & 0 & 0.05 & 0 & 0 & 0 \\ 0 & 1 & 0 & 0 & 0.05 & 0 \\ 0.05 & 0 & 1 & 0 & 0 & 0.1 \\ 0 & 0 & 0 & 1 & 0 & 0 \\ 0 & 0.05 & 0 & 0 & 1 & 0 \\ 0 & 0 & 0.05 & 0 & 0 & 1 \end{bmatrix} \begin{bmatrix} x_0 \\ x_1 \\ x_2 \\ x_3 \\ x_4 \\ x_5 \end{bmatrix} + \begin{bmatrix} 1 \\ 0 \\ 0 \\ 0 \\ 0 \\ 0 \end{bmatrix} u \tag{5.17}$$

For the two-dimensional problem, the control is shown in comparison to the one-dimensional and deterministic cases (Fig. 5.15(a)), as are the coefficients (Fig. 5.15(b)). The MC analysis is given in Fig. 5.16 and demonstrates that uncertainty in the initial condition results in a slightly degraded response due to the dispersion at the

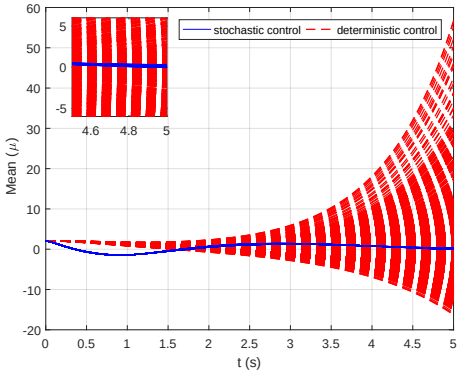

FIGURE 5.14: MC analysis for 1d linear problem.

end (a comparatively higher std of 1.5578, in the two-dimensional case). Despite this, the augmented optimal control solution is still less sensitive to the uncertainties than the deterministic control, as the final expectation and mean is several orders of magnitude smaller than that of the original solution (see Tab. 5.1).

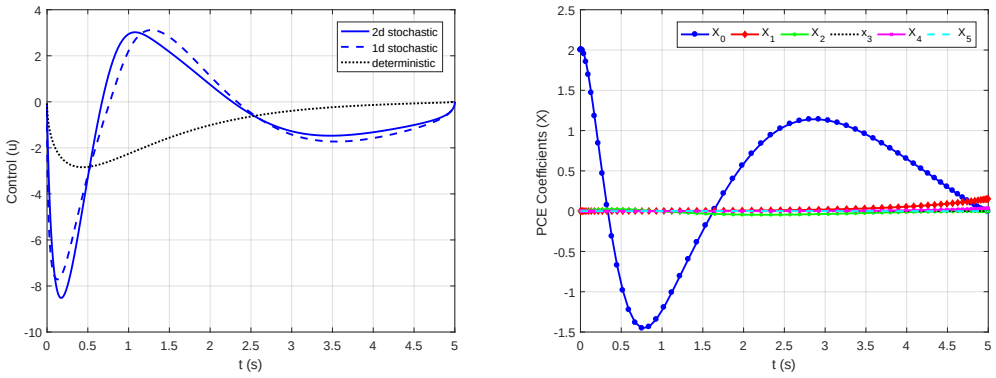

(a) Control for 2d linear problem.

(b) PCE coefficients for 2d linear problem.

FIGURE 5.15: 2d uncertainty: (a) 2d control comparison, and (b) 2d PCE coefficients

A comparison between the solutions obtained for the one and two-dimensional linear problems is presented in Tab. 5.1. Note that the deterministic cost is for the original problem, containing no uncertainty. Thus, the obtained results which show an increase in the cost for the stochastic problem are as expected. Additionally, the optimised stochastic control solution shows a significant reduction in final expectation and variance when compared to the original control; thus, emphasising the benefit of the stochastic AOCP.

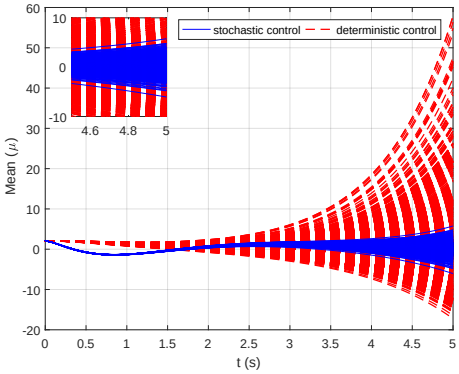

FIGURE 5.16: MC analysis for 2d linear problem.

TABLE 5.1: Comparison of results for 1d and 2d linear problems.

	1d		2d	
Control u	Mean μ	Std σ	Mean μ	Std σ
Deterministic	2.4589	11.8551	2.5556	11.9467
Stochastic	0.0753	0.0308	0.1603	1.5578

5.3 Non-Linear Example

The next example is a non-linear case[47], where the cost function is a initial value Mayer term:

$$\begin{aligned} \min \quad & J = -x(t_f) \\ s.t. \quad & \dot{x}(t) = a(-x(t) + x(t)u(t) - u(t)^2) \\ & x(0) = 1, \quad t_f = [0, 2]s \end{aligned} \tag{5.18}$$

The stochastic quantities are $a \sim N(2.5, 0.1)$ and $x_0 \sim U(0.9, 1.1)$ i.e., normal parameter and uniform initial condition with lower bound, l_b, and upper bound, u_b. For the uniform distribution, $\mu = \frac{1}{2}(l_b + u_b)$ and $\sigma = \frac{1}{2}(u_b - l_b)$. This example differs from the previous, not only in the non-linearity aspect, but also in the fact that the control is affected by the stochastic parameter. The initial parameter coefficients are $\mathbf{a_i} = [2.5, 0.1, 0]$ and the initial conditions are $\mathbf{x_0} = [1, 0, 0]^T$. The augmented stochastic system is therefore:

$$\dot{\mathbf{x}}(t) = -A\mathbf{x}(t) + u(t)A\mathbf{x}(t) - Bu(t)^2 \tag{5.19}$$

In the case of one-dimensional parameter uncertainty,

$$A = \begin{bmatrix} 2.5 & 0.1 & 0 \\ 0.1 & 2.5 & 0.2 \\ 0 & 0.1 & 2.5 \end{bmatrix} \quad \text{and} \quad B = \begin{bmatrix} 2.5 \\ 0.1 \\ 0 \end{bmatrix} \tag{5.20}$$

A comparison of the obtained optimal solution and the original is shown in Fig. 6.12(a) and the corresponding PCE coefficients are shown in Fig. 6.12(b). As before, a MC analysis of 1000 runs is performed in order to establish whether the newly optimised control is more robust in regard to the uncertainty (Fig. 5.18). The stochastic

solution converges to a final expectation of -0.0040 - more than half that of the deterministic case. The solution also exhibits a much higher final convergence (with an std of $8.2893e-05$, compared to 0.0018). Additionally, the stochastic solution actually offers an improved cost function, which is far closer to zero (see Tab. 5.2).

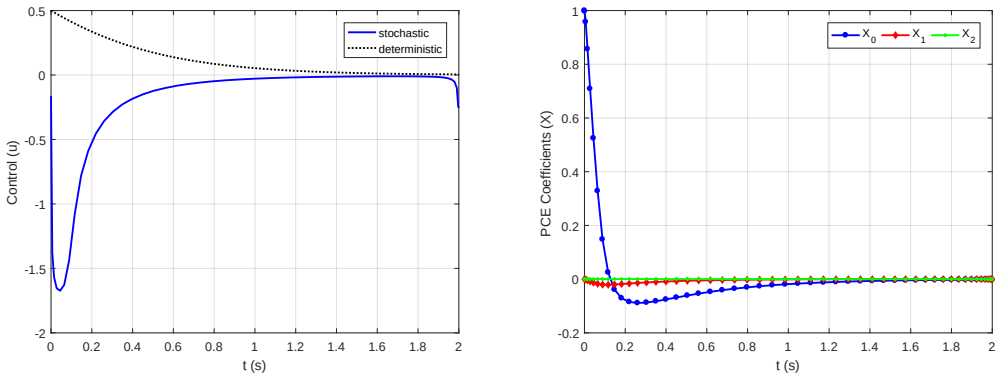

(a) Control for 1d non-linear problem. (b) PCE Coefficients for 1d non-linear problem.

FIGURE 5.17: Control and PCE Coefficients for stochastic non-linear problem (a) 1d control, and (b) 1d PCE coefficients.

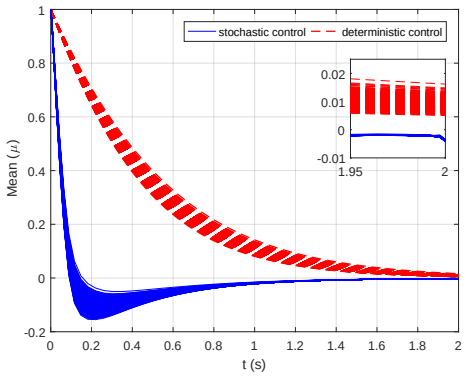

FIGURE 5.18: MC analysis for 1d non-linear problem.

For the two-dimensional case, the transformation matrices are given by Eq. (5.21). The initial PCE coefficients for parameter and initial condition are $\mathbf{a_i} = [2.5, 0, 0.1, 0, 0, 0]$ and $\mathbf{x_0} = [1, 0.1, 0, 0, 0, 0]^T$, respectively.

$$A = \begin{bmatrix} 2.5 & 0 & 0.1 & 0 & 0 & 0 \\ 0 & 2.5 & 0 & 0 & 0.1 & 0 \\ 0.1 & 0 & 2.5 & 0 & 0 & 0.2 \\ 0 & 0 & 0 & 2.5 & 0 & 0 \\ 0 & 0.1 & 0 & 0 & 2.5 & 0 \\ 0 & 0 & 0.1 & 0 & 0 & 2.5 \end{bmatrix} \quad \text{and} \quad B = \begin{bmatrix} 2.5 \\ 0 \\ 0.1 \\ 0 \\ 0 \\ 0 \end{bmatrix} \tag{5.21}$$

The control profile resulting from uncertainties in both the parameter and the initial conditions is shown in Fig. 5.19(a), along with the one-dimensional and deterministic cases. The corresponding PCE coefficients are given in Fig. 5.19(b). Again it

is noted that there are six coefficients due to the fact that it is a second order expansion, with two stochastic variables. The uncertainty in initial condition is very obvious in both the stochastic and deterministic case, however, the former converges very nicely to a final expectation of $-4.7401e-04$ due to this larger expansion. A full comparison of the statistics for the one-dimensional and two-dimensional non-linear problems is shown in Tab. 5.2.

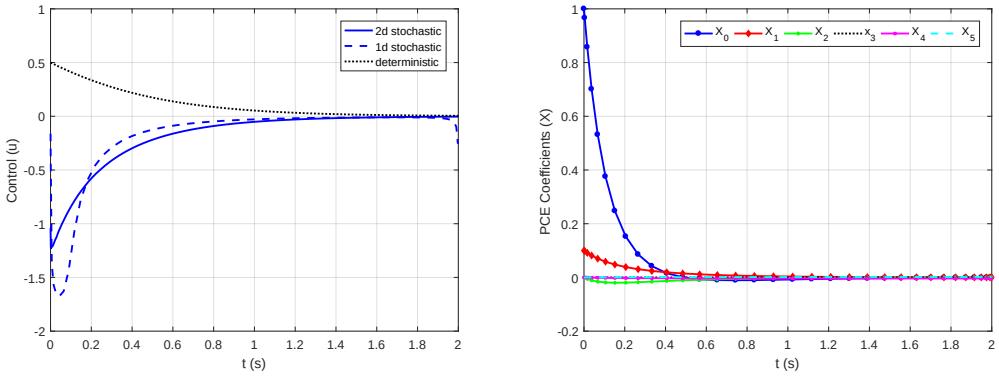

(a) Control for 2d non-linear problem.

(b) PCE Coefficients for 2d non-linear problem.

FIGURE 5.19: Control and PCE Coefficients for stochastic non-linear problem (a) 2d control, and (b) 2d PCE coefficients.

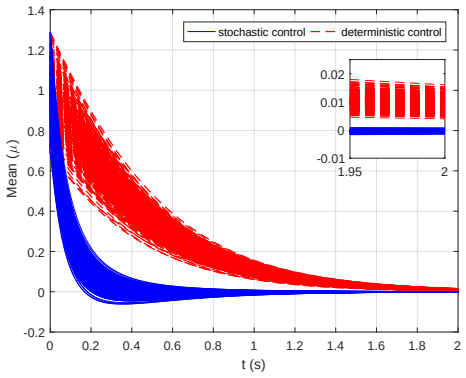

FIGURE 5.20: MC analysis for 2d non-linear problem.

TABLE 5.2: Comparison of results for 1d and 2d non-linear problems.

	1d		2d	
Control u	Mean μ	Std σ	Mean μ	Std σ
Deterministic	0.0091	0.0018	0.0092	0.00210
Stochastic	-0.0040	8.2893e-05	-4.7401e-4	3.3636e-04

5.4 Hyper-sensitive Problem

A hyper-sensitive problem can be characterised as having three well defined segments: take-off, cruise, and landing. The so-called take-off and landing phases are dependent on the boundary conditions, whilst cruise is subject to the system dynamics and the cost function. The OCP is deemed hyper-sensitive if the final time is much larger in comparison to the contraction and expansion rates of the Hamiltonian system[48]. An increase in final time will results in a longer cruise segment, in which the state is minimised[49].

The OCP is defined as such[28]:

$$\begin{aligned} \min \quad & J = \int \frac{1}{2}(x^2 + u^2) \\ s.t. \quad & \dot{x}(t) = -ax(t)^3 + u(t) \\ & x(0) = 1.5, x(t_f) = 1 \quad t = [0, 50]s \end{aligned} \tag{5.22}$$

The stochastic system is then concerned with uniform uncertainty on the parameter, $a \sim U(0.2, 1.8)$. This example varies from those covered previously due to the non-linearity in the state dynamics. Consequently, the PCE will consist of two additional basis functions, $\psi(\xi)$.

$$\dot{x}_k(t) = -\frac{1}{< \psi_k^2(\xi) >} < \sum_{i=0}^{P} a_i(t)\psi_i(\xi) \left(\sum_{j=0}^{P} x_j(t)\psi_j(\xi) \right)^3 , \psi_k(\xi) > \tag{5.23}$$

This is equivalent to:

$$\dot{x}_m(t) = -\frac{1}{< \psi_m^2(\xi) >} < \sum_{i=0}^{P}\sum_{j=0}^{P}\sum_{k=0}^{P}\sum_{l=0}^{P} a_i(t)\psi_i(\xi)x_j(t)\psi_j(\xi)x_k(t)\psi_k(\xi)x_l(t)\psi_l(\xi), \psi_m(\xi) > \tag{5.24}$$

The polynomial basis is thus the tensor product of 5 Legendre polynomials of the order corresponding to the respective single index. For a second order expansion $P = 3$. The initial PCE coefficients for the parameter as therefore $\mathbf{a_i} = [1, 0.8, 0]$, and the initial condition PCE coefficients are $\mathbf{x_0} = [1.5, 0, 0]^T$. The PCE will result in an augmented matrix, A, of dimension $[3 \times 27]$. Consequently, the Kronecker product of the state, $\mathbf{x}$, must also be taken to results in a $[27 \times 1]$ vector. This is demonstrated by Eq. (5.25), where x_k denotes the Kronecker product of the state PCE coefficients.

$$\mathbf{x_k} = \mathbf{x} \otimes (\mathbf{x} \otimes \mathbf{x}) \tag{5.25}$$

The control profile obtained for the optimised stochastic system is presented in Fig. 5.21(a), and it can be seen that the uncertainty affects the control input in the initial value and also the final value, however, the minimised profile is maintained and is in agreement with previous work[28]. The original trajectory and the expectation of the new stochastically optimal trajectory is depicted in Fig. 5.21(b).

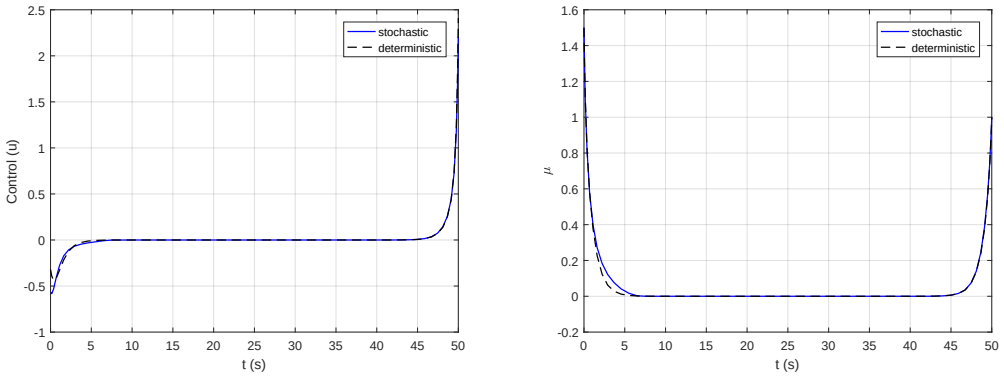

(a) Control for hyper-sensitive problem (b) Expectation of hyper-sensitive problem

FIGURE 5.21: Control and expectation for 1d hyper-sensitive problem

The corresponding PCE coefficients are presented in Fig. 5.22. As expected, the first coefficient demonstrates the characteristic of the minimised state - maintaining a minimum throughout the majority of the time.

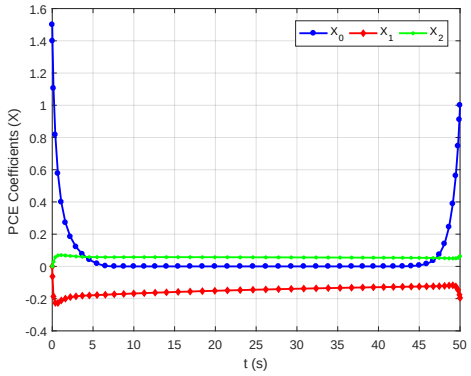

FIGURE 5.22: PCE coefficients for 1d hyper-sensitive problem

If we now compare the expectation i.e. the first augmented state to the deterministic state, it is obvious that the stochastic system is optimised (Fig. 5.21(b)).

Considering that for this example, the cost function includes the control, the manner in which the effectiveness of the stochastic solution is determined is slightly different. First of all, the stochastic cost is the Lagrange term (previous examples have been concerned purely with the Mayer term), and second of all, it is not merely the case of minimising the expectation of the state. Instead, for the MC analysis the cost function is evaluated using the deterministic and stochastic control solutions. This was performed for 1000 runs, which is depicted in Fig. 5.23.

TABLE 5.3: Statistics for 1d hyper-sensitive problem

Control u	Final Cost J(t_f)
Deterministic	3.2578
Stochastic	3.0819

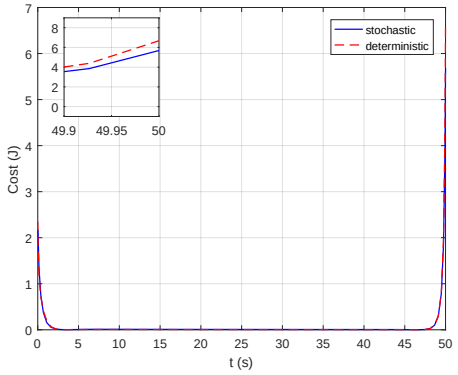

FIGURE 5.23: MC analysis for 1d hyper-sensitive problem

5.5 Double Integrator

This example introduces the manner in which the stochastic augmented system is derived for a Multi-Input, Multi-Output (MIMO) system. The OCP is to minimise the final value of the first state, x_1. The deterministic problem is therefore defined as follows:

$$\begin{aligned} \min \quad & J = \|x_1(t)\| \\ s.t. \quad & \dot{x}_1(t) = x_2(t) \\ & \dot{x}_2(t) = ax_1(t) + u(t) \\ & x(0) = [2, 1] \\ & x_1(t_f) = 0 \quad t = [0, 10]s \end{aligned} \tag{5.26}$$

where the parameter, $a = 1$ in the case of no uncertainty.

If we then introduce uncertainty to the parameter of distribution $a \sim N(1, 0.15)$ with an expansion of $n = 2$, each state consists of 3 PCE terms, and the initial conditions for the PCE are $\mathbf{a_i} = [1, 0.015, 0]$, $\mathbf{x_{10}} = [2, 0, 0]^T$ and $\mathbf{x_{20}} = [1, 0, 0]^T$. The PCE for parameter uncertainty in is shown by Eq. 5.27

$$\begin{aligned} \dot{\mathbf{x}}(t)_{1,k} &= x_{2,k}(t) \\ \dot{\mathbf{x}}(t)_{2,k} &= \frac{1}{< \psi_k^2(\xi) >} \sum_{i=0}^{P} \sum_{j=0}^{P} a_i(t) x_{1,j}(t) \psi_i(\xi) \psi_j(\xi) + u(t), \psi_k(\xi) > \end{aligned} \tag{5.27}$$

The stochastic cost function is a minimum expectation Mayer problem given by

$$J = \mathbb{E}[x_1(t)] \tag{5.28}$$

Following evaluation of the integrals, e_{ijk}, and the inner products, γ_k, the simplified stochastic augmented system is determined:

$$\begin{aligned} \dot{\mathbf{x}}_\mathbf{1}(t) &= A_2 \mathbf{x_2}(t) \\ \dot{\mathbf{x}}_\mathbf{2}(t) &= A_1 \mathbf{x_1}(t) + Bu(t) \end{aligned} \tag{5.29}$$

where,

$$A_1 = \begin{bmatrix} 1 & 0.15 & 0 \\ 0.15 & 1 & 0.3 \\ 0 & 0.15 & 1 \end{bmatrix} \quad A_2 = \begin{bmatrix} 1 & 0 & 0 \\ 0 & 1 & 0 \\ 0 & 0 & 1 \end{bmatrix} \quad \text{and} \quad B = \begin{bmatrix} 1 \\ 0 \\ 0 \end{bmatrix} \tag{5.30}$$

Remark 4 It is important to note that the expansion for deterministic states will always consist of an expansion as given by Eq. (3.7) with $a_i = 1$ i.e. parameter and $x_0 = [\mu_x, 0, ..., 0]^T$.
The new stochastic control solution obtained from these dynamics is shown in Fig. 5.24.

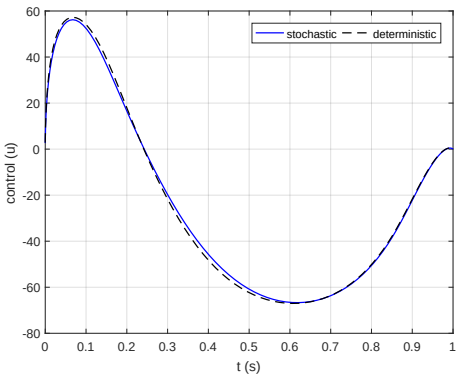

FIGURE 5.24: Control for $1d$ double integrator problem, $n = 2$

The PCE coefficients for the states x_1 and x_2 are shown in Figs. 5.25(a) and 5.25(a), respectively. The expectation or mean, μ is given by the coefficient X_0 and it can be seen that the minimum expectation of the first state is reached - as was specified in the stochastic cost function given by Eq. (5.28).

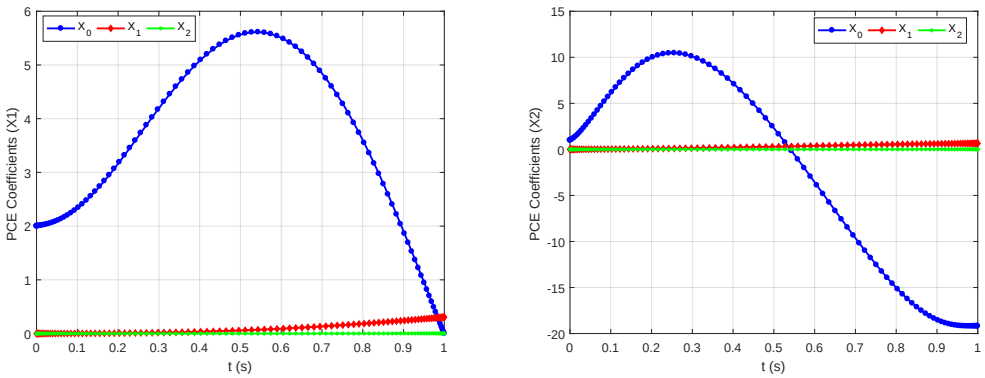

(a) PCE coefficients for x_1

(b) PCE coefficients for x_2

FIGURE 5.25: PCE coefficients for $1d$ double integrator problem, $n = 2$

Next, MC analysis is performed for 1000 runs (Fig. 5.26) to provide a comparison between the stochastic and deterministic control solutions. The aim is to establish whether the new solution does in fact result in the minisation of the first state, when subject to this uncertainty. The results are summarised in Tab. 5.4):

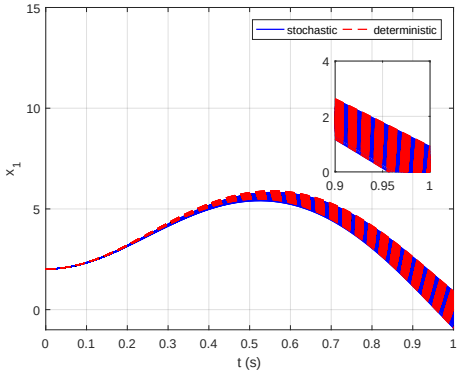

FIGURE 5.26: MC analysis for $1d$ double integrator problem, $n = 2$

TABLE 5.4: Comparison of final state for $1d$ parameter uncertainty, $n = 2$

Problem	Mean μ	Std σ
Deterministic	0.0043	0.3106
Stochastic	0.0010	0.3069

From Tab. 5.4 it is clear that the stochastic solution offers a reduction in the expectation of the state. However, an improvement can still be made by increasing the order of expansion. Therefore we will now consider a PCE of $n = 4$. The control profile obtained by the higher order expansion is given in Fig. 5.27 and shows a greater difference in comparison to the deterministic control i.e. the higher the order, the greater the difference between the two profiles. This is followed by the PCE coefficients in Figs. 5.28(a) and 5.28(b).

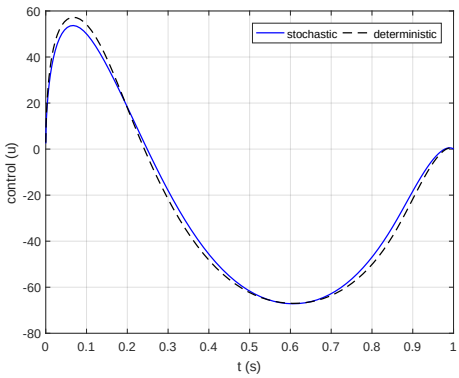

FIGURE 5.27: Control for $1d$ double integrator problem, $n = 4$

Upon first glance, the MC analysis looks very similiar to the previous, however, a reduction of the expectation has indeed been achieved. This is depicted in Tab. 5.5.

So the AOCP thus far has been for minimum expectation, as dictated by the original cost function. However, from the MC analysis obtained, it is quite obvious that the standard deviation is very high for both control solutions. Now we will demonstrate the effect of including standard deviation in the cost function (see Ch. 4 and Eq. 4.1).

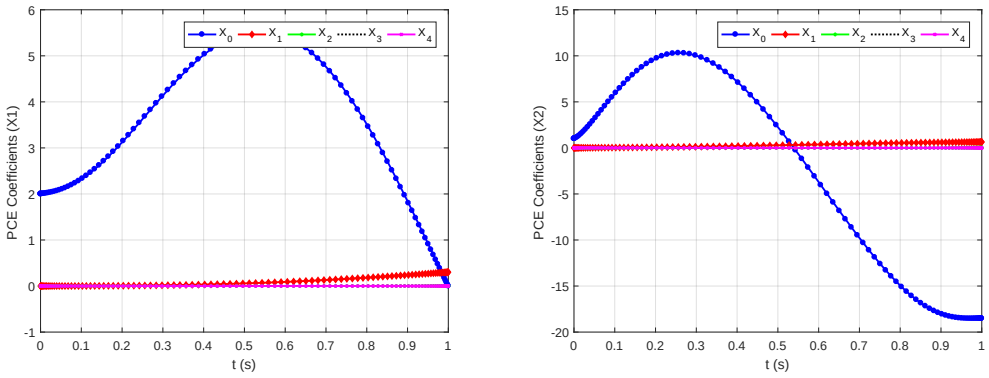

(a) PCE coefficients for x_1 (b) PCE coefficients for x_2

FIGURE 5.28: PCE coefficients for $1d$ double integrator problem, $n = 4$

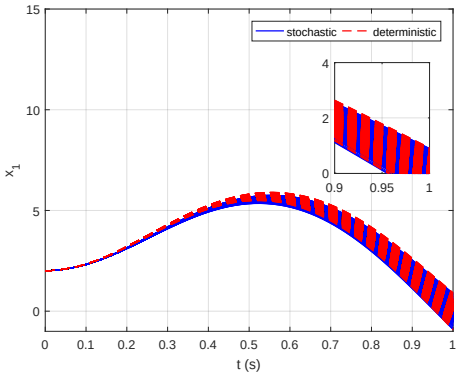

FIGURE 5.29: MC analysis for $1d$ double integrator problem, $n = 4$

TABLE 5.5: Comparison of final state for $1d$ parameter uncertainty, $n = 4$

Problem	Mean μ	Std σ
Deterministic	0.0043	0.3106
Stochastic	9.9451e-04	0.3034

The PCE coefficients shown in Figs. 5.30(a) and 5.30(b) differ from those obtained previously in that the expectation is reduced quite drastically. The response for the x_1 augmented terms is desirable, however, you can see the response of x_2 is quite sharp. After all, the second state is not specified in the stochastic cost function and is the derivative of ther terms shown in Fig. 5.30(a).

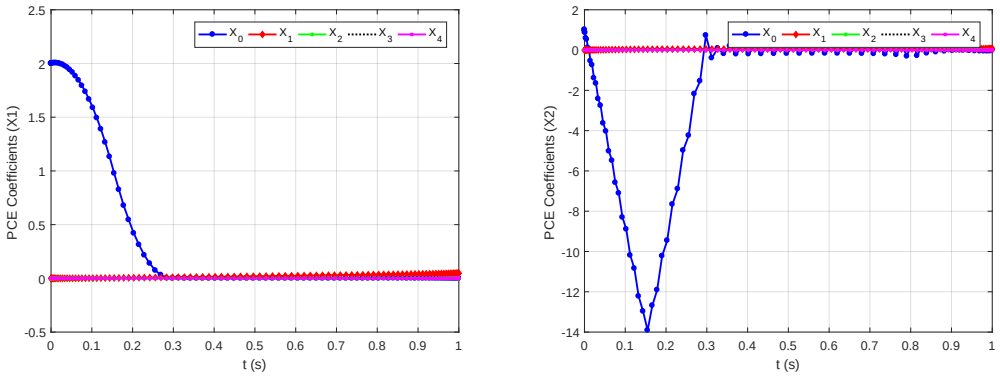

(a) PCE coefficients for x_1 (b) PCE coefficients for x_2

FIGURE 5.30: PCE coefficients for $1d$ double integrator problem, $n = 4$ (minimum std)

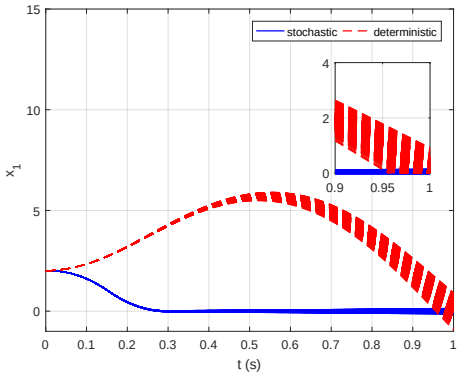

FIGURE 5.31: MC analysis for $1d$ double integrator problem, $n = 4$ (minimum std)

The MC analysis shows a drastic difference in the convergence of the solution. Evidently, the standard deviation of the trajectory has been reduced considerably. A comparison of results for the new minimum expectation and standard deviation profile is shown in Tab. 5.6.

TABLE 5.6: Comparison of final state for $1d$ parameter uncertainty, $n = 4$ (minimum std)

Problem	Mean μ	Std σ
Deterministic	0.0043	0.3106
Stochastic	-0.0037	0.0485

Chapter 6

Validation of Polynomial Chaos Expansions

6.1 PCET Toolbox

In order to validate the PCE obtained via the Galerkin Projection method, the PCET (Polynomial Chaos Expansion Toolbox) was used. This is a MATLAB-based toolbox that has been developed at Technische Universität Chemnitz[46;50]. It has been developed for application to stochastic non-linear control systems, and is capable of performing uncertainty propagation and parameter estimation. This is achieved by Galerkin Projection or Stochastic Collocation, and it also offers MC analysis. In the early development of this work, it offered a very important verification step. PCET employs the symbolic toolbox within MATLAB to perform the PCE, however, the process in SPARTAN does not require any additional toolbox.

6.2 Example Zero

This is the first problem that was validated using PCET. As previously defined in Ch. 5, the one-dimensional problem given by Eq. (5.1) and presented here concerns uncertainty in the parameter with a distribution $a \sim N(0,1)$. First, we consider the problem for $n = 2$. The resultant 3 PCE coefficients are given for both SPARTAN and PCET:

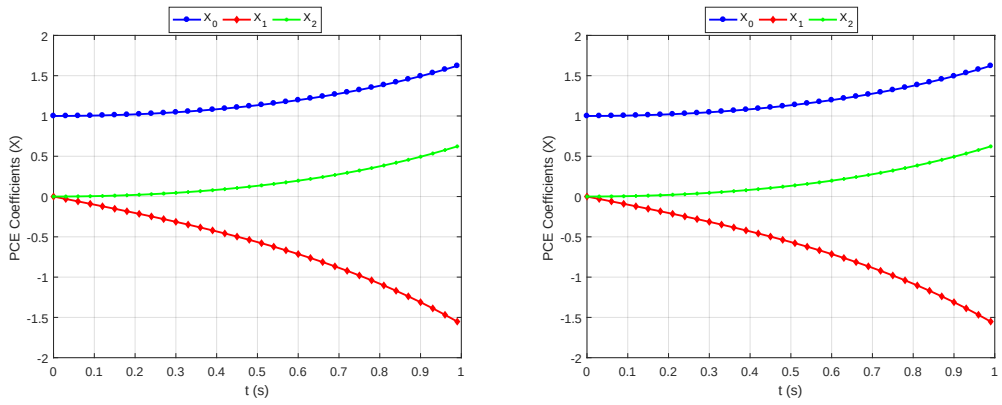

(a) SPARTAN PCE coefficients for $1d$ Example Zero.

(b) PCET PCE coefficients for $1d$ Example Zero.

FIGURE 6.1: PCE coefficients for $1d$ Example Zero (n=2) (a) SPARTAN, and (b) PCET.

The mean, or expectation, $\mathbb{E}[x]$, is given by 6.2(a), whilst the standard deviation is presented by 6.2(b). Both demonstrate full agreement between SPARTAN and PCET, however, it is noticeable that the standard deviation, σ, is not matching the analytical value, whilst the MC of 7000 runs does. This is due to the fact that when dealing with a complex system, the system is better represented by a higher order expansion. Despite this, both SPARTAN and PCET agree.

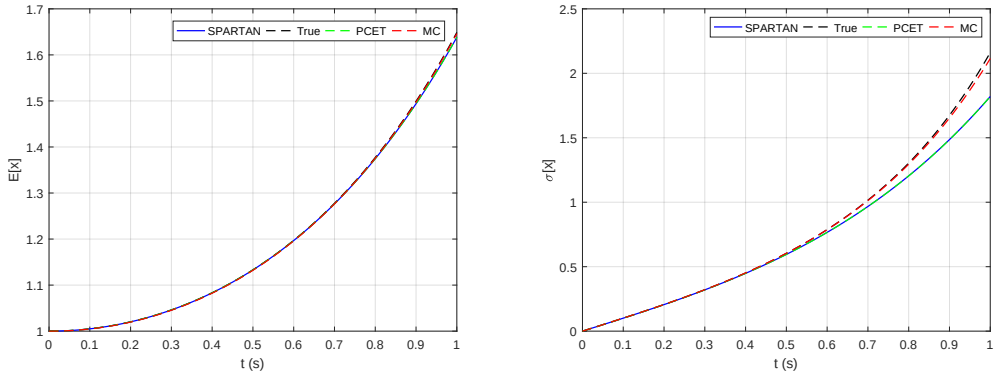

(a) Mean of 2^{nd} order Example Zero

(b) Std of 2^{nd} order Example Zero

FIGURE 6.2: Statistics for $1d$ Example Zero (n = 2) (a) mean, and (b) std.

In order to demonstrate this, an expansion of $n = 4$ was also performed. The augmented system thus consists of 5 PCE coefficients, which are depicted in Figs. 6.3(a) and 6.3(b). Again, SPARTAN and PCET convey identical results, which now match the true solution. These results also demonstrate a higher accuracy that that achieved with the MC (Figs. 6.4(a) and 6.4(b)).

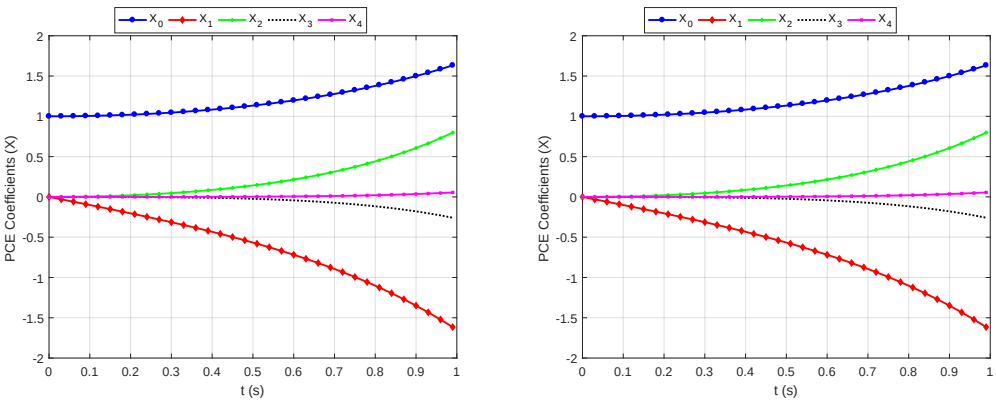

(a) SPARTAN PCE coefficients for $1d$ Example Zero.

(b) PCET PCE coefficients for $1d$ Example Zero.

FIGURE 6.3: PCE coefficients for $1d$ Example Zero (n=4) (a) SPARTAN, and (b) PCET.

Next, multi-dimensional uncertainty is considered, and which has mixed distributions. The parameter $a \sim N(0, 1)$, whilst the initial condition is uniform - $x_0 \sim U(0.4, 1.6)$. There are thus 6 PCE coefficients for $n = 2$ and they are shown in Figs. 6.5(a) and

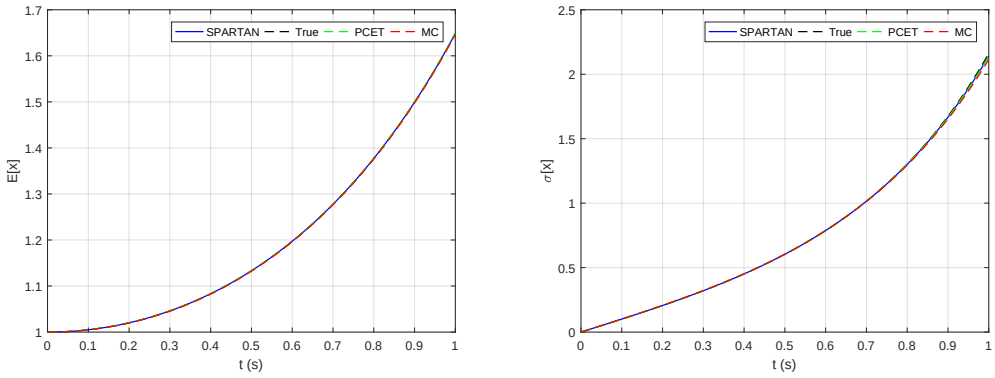

(a) Mean of 4^{th} order for Example Zero

(b) Std of 4^{th} order for Example Zero

FIGURE 6.4: Statistics for $1d$ Example Zero (n = 4) (a) mean (b) std.

6.5(b). The corresponding statistics are depicted by Figs. 6.6(a) and 6.6(b). The solutions of SPARTAN and PCET are identical as before, and full convergence with the analytical solution is achieved by increasing n.

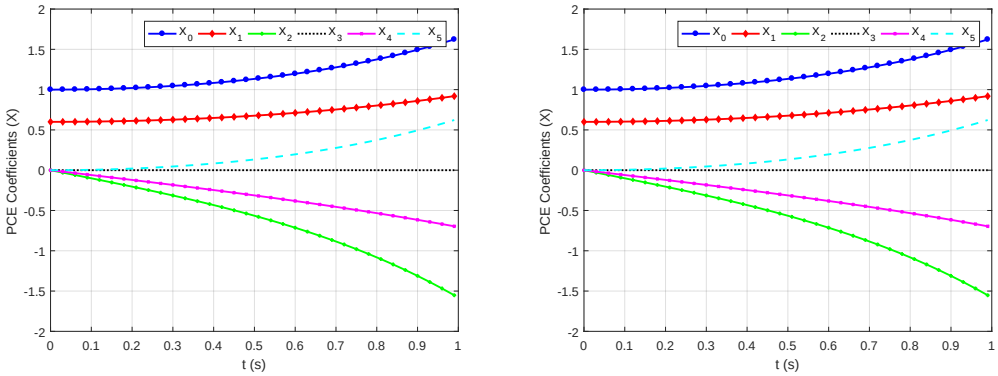

(a) SPARTAN PCE coefficients for $2d$ Example Zero.

(b) PCET PCE coefficients for $2d$ Example Zero.

FIGURE 6.5: PCE coefficients for $2d$ Example Zero (n=4) (a) SPARTAN, and (b) PCET.

6.3 Non-linear Example

Next, a non-linear example is considered. It is important to make a distinction here - non-linearity occurs in the dynamics and/or the uncertainties. For instance, the problem given by Eq. 6.1 includes the former, since we will only consider a single uncertainty $(d = 1)$. However, the PCE is multi-dimensional due to the higher-dimensional term. This was demonstrated in the optimisation of the Hyper-sensitive problem (i.e x^3). Now if we consider it purely in terms of the PCE, the system is represented as such:

$$\dot{x}(t) = -ax(t)^3 \tag{6.1}$$

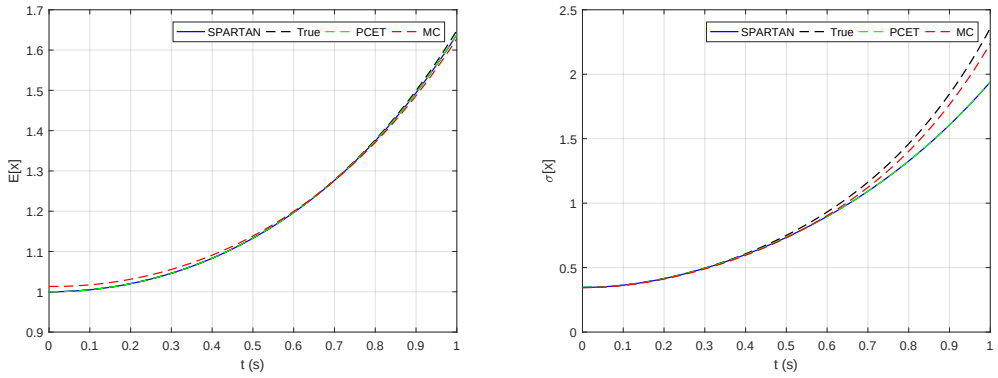

(a) Mean of $2d$ Example Zero (b) Std of $2d$ Example Zero

FIGURE 6.6: Statistics for $2d$ Example Zero (n = 2) (a) mean, and (b) std.

Uncertainty is placed upon the parameter with a uniform distribution $a \sim U(0.2, 0.8)$. It is now trivial to note that for a $1d$ expansion, there are $n + 1$ coefficients. The resultant augmented matrix, A, is of dimension $[3 \times 27]$ and is identical for both SPARTAN and PCET. These coefficients are shown in Figs. 6.7(a) and 6.7(b).

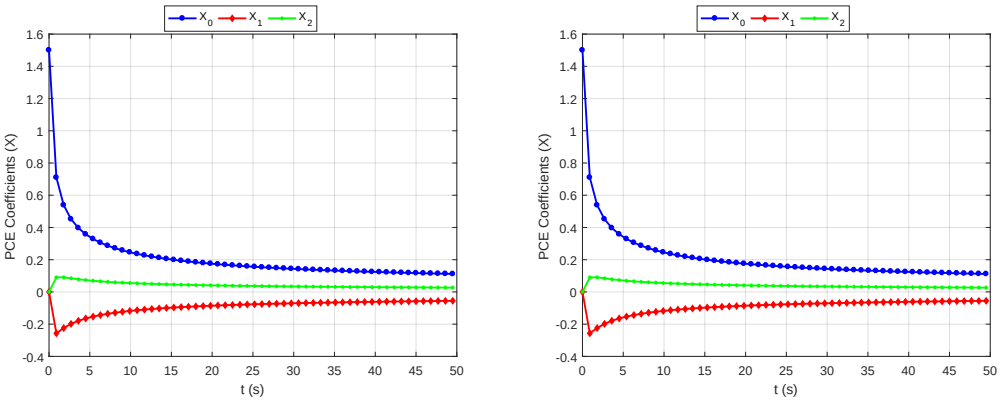

(a) PCE coefficients for Non-linear problem (b) PCE coefficients for Non-linear problem

FIGURE 6.7: PCE coefficients for Non-linear problem (n = 2) (a) SPARTAN, and (b) PCET.

The statistics that are subsequently deduced are therefore again equivalent for both SPARTAN and PCET. The mean and standard deviation of the MC demonstrated a very slight deviation for 1000 runs, however, they are equivalent for 2000 runs (as shown in Fig. 6.8(b)).

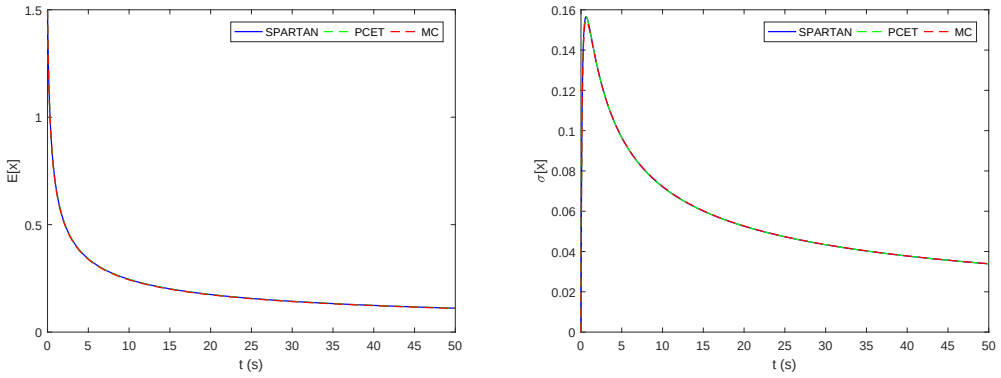

(a) Mean of Non-linear problem

(b) Std of Non-linear problem

FIGURE 6.8: Statistics for Non-linear problem (n=2). (a) mean, and (b) std

6.4 Lorenz Attractor

The final example presented here within the validation process is that of the Lorenz attractor - a problem that originates in the field of fluid dynamics. The original system exhibited chaotic behaviour - vast differences were obtained when small changes were made to the initial conditions. This is considered one of the earliest observations of the Butterfly Effect[51]. This set of coupled non-linear differential equations can lead to some interesting trajectories. The deterministic solution is depicted by Fig. 6.9.

$$\begin{aligned} \dot{x}_1(t) &= \sigma(x_2(t) - x_1(t)) \\ \dot{x}_2(t) &= x_1(t)(\rho - x_3(t)) - x_2(t) \\ \dot{x}_3(t) &= x_1(t)x_2(t) - \alpha x_3(t) \\ x(0) &= [1.5, -1.5, 25.5]^T, \quad \sigma = 10, \rho = 28, \alpha = 2.667 \end{aligned} \tag{6.2}$$

Now for the uncertainty analysis, the multi-dimensional case is performed in which each parameter is stochastic. First, each parameter is given a normal distribution, with $\sigma = 0.1$. Consequently, the overall order of expansion is $P = 10$, which dictates the number of PCE coefficients for each augmented state. The expansion of states, x, are shown in Figs. 6.11(a) - 6.11(f), respectively. The resultant expectation and standard deviation of each state is depicted in Figs. 6.10(a) and 6.10(b):

The problem was then performed using $n = 4$, considering that the MC diverges a little towards the end. This again demonstrated a slight difference for the first state, however, the solution from SPARTAN and PCET are in agreement with the expected solution as covered by Bhattachayra[52]. The number of MC runs was increased from 1000 to 10000, but the same solution was achieved. Due to the fact that the MC simulation output from PCET also had the same issue, it can be inferred that a relatively small MC campaign is unable to capture this system as accurately as that of PC.

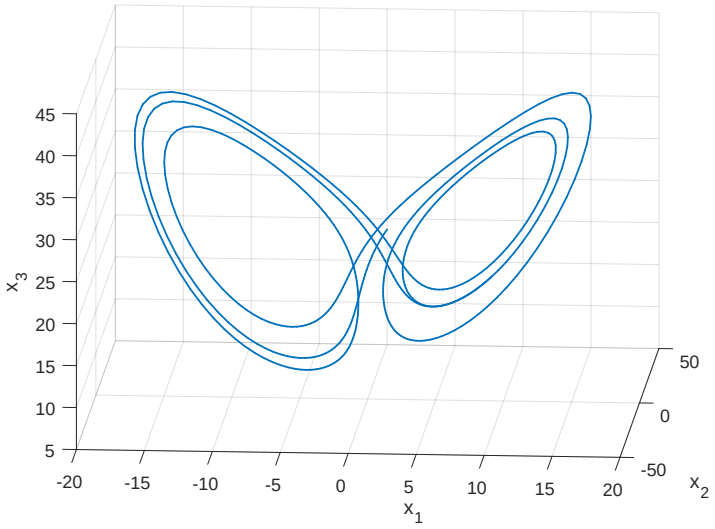

FIGURE 6.9: Deterministic solution of Lorenz Attractor.

For this example, it is important to note that PCET employs a slightly different Graded Lexicographic multi-indexing method than employed here[4], which means that for $d > 2$, the entries in the augmented matrix, A, will be positions in a slightly different manner however this does not impact the solution in any way.

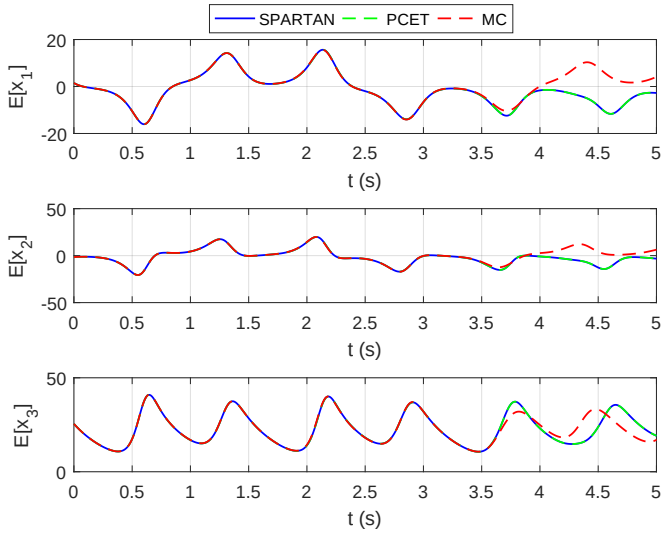

(a) Mean of Lorenz attractor problem.

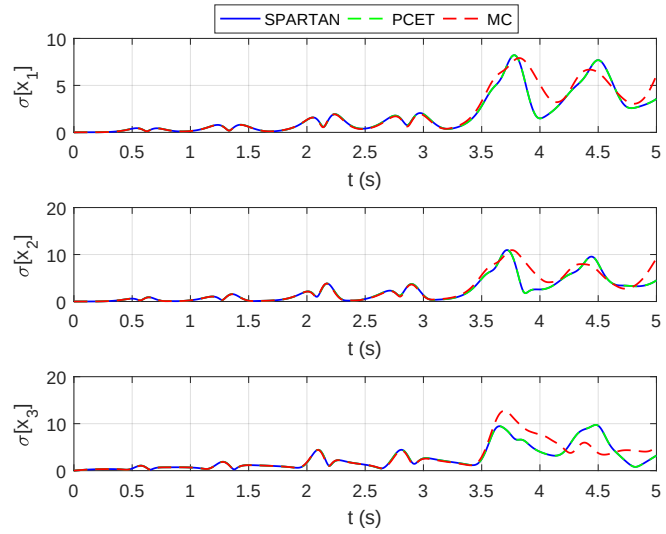

(b) Std of Lorenz attractor problem.

FIGURE 6.10: Statistics for Lorenz attractor problem (n = 2) (a) mean, and (b) std.

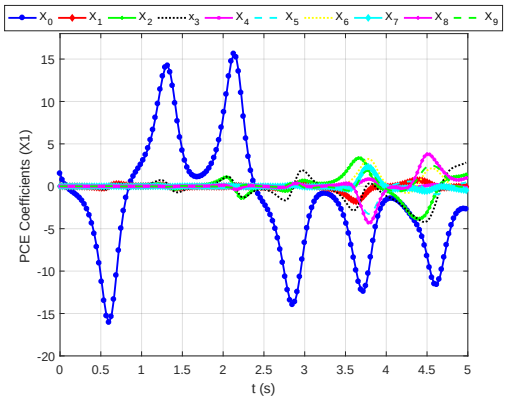

(a) PCE coefficients for x_1 of 2^{nd} order Lorenz problem

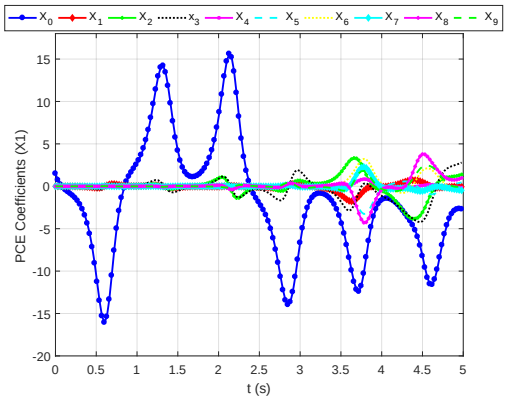

(b) PCE coefficients for x_1 of 2^{nd} order Lorenz problem

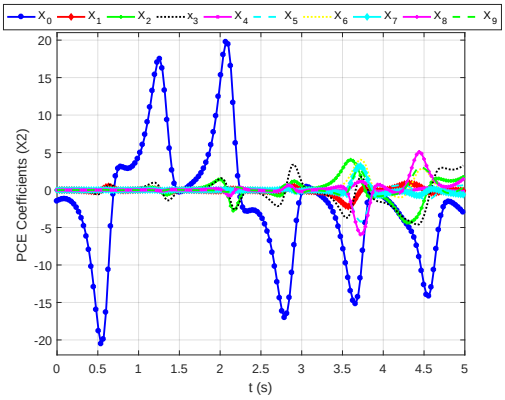

(c) PCE coefficients for x_2 of 2^{nd} order Lorenz problem

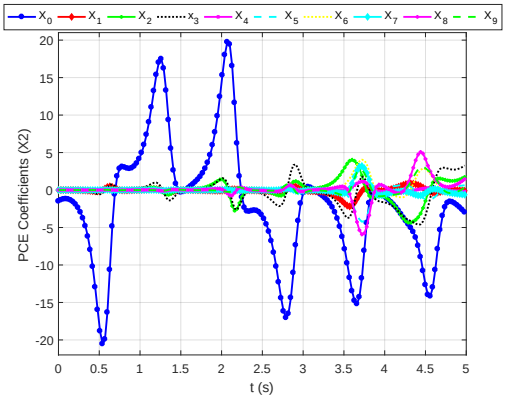

(d) PCE coefficients for x_2 of 2^{nd} order Lorenz problem

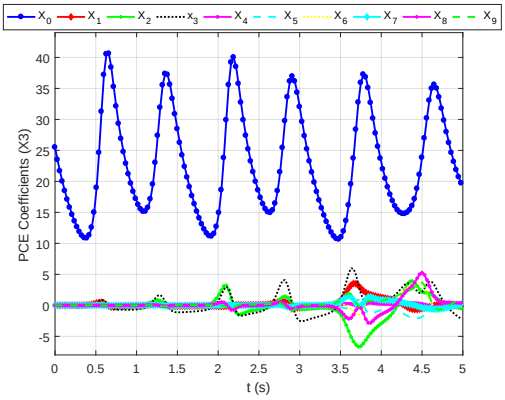

(e) PCE coefficients for x_3 of 2^{nd} order Lorenz problem

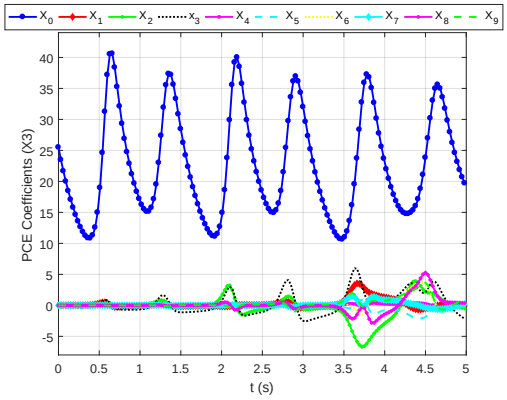

(f) PCE coefficients for x_3 of 2^{nd} order Lorenz problem

FIGURE 6.11: PCE coefficients for Lorenz attractor problem (n = 2) (a) SPARTAN x_1 (b) PCET x_1 (c) SPARTAN x_2 (d) PCET x_2 (e) SPARTAN x_3, and (f) PCET x_3 .

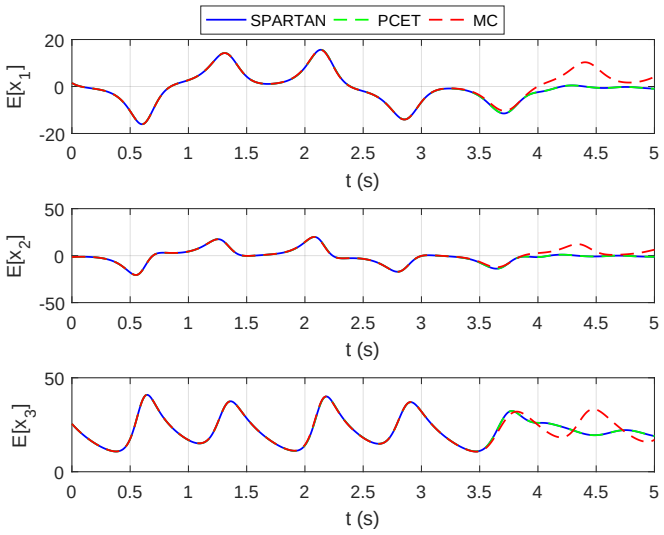

(a) Mean of Lorenz attractor problem.

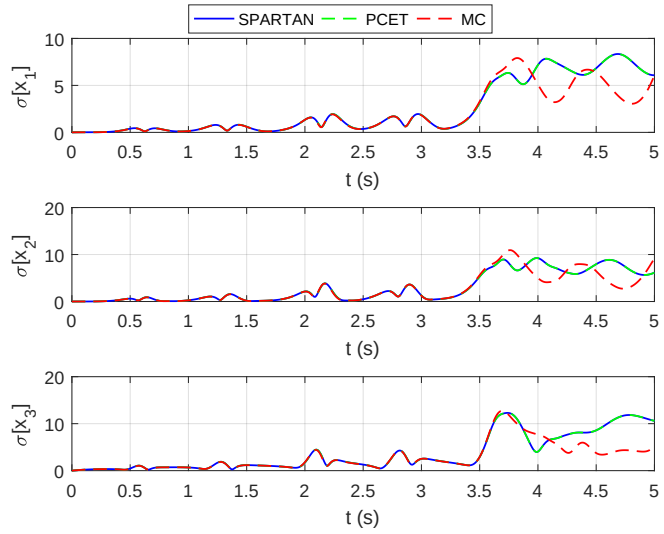

(b) Std of Lorenz attractor problem.

FIGURE 6.12: Statistics for Lorenz attractor problem (n = 4) (a) mean (b) std.

Chapter 7

Conclusions

It has been demonstrated how to obtain optimal trajectories in the presence of uncertainties. Multivariate polynomial chaos is a very effective method for uncertainty propagation, offering accurate results without heavy computational implications. Uncertainty modelling was performed using the PCE method, and the Galerkin projection was used in order to transform the stochastic system into the augmented deterministic equivalent.

The original cost functions were transformed into their corresponding stochastic equivalent, in which we are able to manipulate quantities such as mean and standard deviation. The resultant deterministic system was subsequently solved using NLP transcription, performed by SPARTAN, in order to obtain the stochastic optimal trajectory. These principles were demonstrated by a variety of numerical examples. This demonstrated the capability to analyse multi-dimensional, mixed distribution problems. This has been done in order to convey the benefits of gPC in application to stochastic optimal trajectory generation problems. Results clearly show an improvement in performance with respect to deterministic classic approach of several orders of magnitude.

The implementation of the PCE method is currently able to analyse problems containing up to 5 random quantities and non-linear dynamics terms up to the 7^{th} order, however, it has been developed in a manner that will make any extension to this simple. Future work will include improving the automatic nature of the analysis; particularly in terms of the interface with SPARTAN. This will lead to the ability to solve much more complex systems. It would also be interesting to extend the distributions that can be modelled by this framework, and not be limited to only Gaussian and Uniform stochastic variables.

Appendix A

Polynomial Chaos Expansion for one dimensional Linear System

The derivation presented here represents a one-dimensional uncertainty for linear systems. Due to the univariate nature of the problem, the order of expansion is simply related to the highest order of polynomial, i.e. $n+1$. If we consider a second order expansion, there there will be three resulting PCE coefficients in the augmented system and hence, A is a $[3 \times 3]$ matrix. The subscript of each univariate polynomial base, ψ, is the single index, i, j, k, respectively and conveys the order of the polynomial.

$$\dot{\mathbf{x}} = \begin{bmatrix} \dot{x}_0 \\ \dot{x}_1 \\ \dot{x}_2 \end{bmatrix} = \begin{bmatrix} A_{00} & A_{01} & A_{02} \\ A_{10} & A_{11} & A_{12} \\ A_{20} & A_{21} & A_{22} \end{bmatrix} \begin{bmatrix} x_0 \\ x_1 \\ x_2 \end{bmatrix} \tag{A.1}$$

where,

$$\dot{x}_0 \quad \text{terms} \quad \begin{cases} \gamma_0 &= < \psi_0^2(\xi) > \; = \int \psi_0(\xi)\psi_0(\xi) \\ A_{00} &= \frac{1}{\gamma_0}[a_0 \int \psi_0(\xi)\psi_0(\xi)\psi_0(\xi) + a_1 \int \psi_1(\xi)\psi_0(\xi)\psi_0(\xi) + a_2 \int \psi_2(\xi)\psi_0(\xi)\psi_0(\xi)] \\ A_{01} &= \frac{1}{\gamma_0}[a_0 \int \psi_0(\xi)\psi_1(\xi)\psi_0(\xi) + a_1 \int \psi_1(\xi)\psi_1(\xi)\psi_0(\xi) + a_2 \int \psi_2(\xi)\psi_1(\xi)\psi_0(\xi)] \\ A_{02} &= \frac{1}{\gamma_0}[a_0 \int \psi_0(\xi)\psi_2(\xi)\psi_0(\xi) + a_1 \int \psi_1(\xi)\psi_2(\xi)\psi_0(\xi) + a_2 \int \psi_2(\xi)\psi_2(\xi)\psi_0(\xi)] \end{cases} \tag{A.2}$$

$$\dot{x}_1 \quad \text{terms} \quad \begin{cases} \gamma_1 &= < \psi_1^2(\xi) > \; = \int \psi_1(\xi)\psi_1(\xi) \\ A_{10} &= \frac{1}{\gamma_1}[a_0 \int \psi_0(\xi)\psi_0(\xi)\psi_1(\xi) + a_1 \int \psi_1(\xi)\psi_0(\xi)\psi_1(\xi) + a_2 \int \psi_2(\xi)\psi_0(\xi)\psi_1(\xi)] \\ A_{11} &= \frac{1}{\gamma_1}[a_0 \int \psi_0(\xi)\psi_1(\xi)\psi_1(\xi) + a_1 \int \psi_1(\xi)\psi_1(\xi)\psi_1(\xi) + a_2 \int \psi_2(\xi)\psi_1(\xi)\psi_1(\xi)] \\ A_{12} &= \frac{1}{\gamma_1}[a_0 \int \psi_0(\xi)\psi_2(\xi)\psi_1(\xi) + a_1 \int \psi_1(\xi)\psi_2(\xi)\psi_1(\xi) + a_2 \int \psi_2(\xi)\psi_1(\xi)\psi_1(\xi)] \end{cases} \tag{A.3}$$

$$\dot{x}_2 \quad \text{terms} \quad \begin{cases} \gamma_2 &= < \psi_2^2(\xi) > \; = \int \psi_2(\xi)\psi_2(\xi) \\ A_{20} &= \frac{1}{\gamma_2}[a_0 \int \psi_0(\xi)\psi_0(\xi)\psi_2(\xi) + a_1 \int \psi_1(\xi)\psi_0(\xi)\psi_2(\xi) + a_2 \int \psi_2(\xi)\psi_0(\xi)\psi_2(\xi)] \\ A_{21} &= \frac{1}{\gamma_2}[a_0 \int \psi_0(\xi)\psi_1(\xi)\psi_2(\xi) + a_1 \int \psi_1(\xi)\psi_0(\xi)\psi_2(\xi) + a_2 \int \psi_2(\xi)\psi_0(\xi)\psi_2(\xi)] \\ A_{22} &= \frac{1}{\gamma_2}[a_0 \int \psi_0(\xi)\psi_2(\xi)\psi_2(\xi) + a_1 \int \psi_1(\xi)\psi_2(\xi)\psi_2(\xi) + a_2 \int \psi_2(\xi)\psi_2(\xi)\psi_2(\xi)] \end{cases} \tag{A.4}$$

Note that the third component in each A term is zero since the PCE coefficient matrix is $a_i = [\mu_a, \sigma_a, 0]$ for one-dimensional parameter uncertainty. It also follows that these relationships are further simplified for the case of initial condition uncertainty due to the fact that the only non-zero initial PCE coefficient is μ_a.

Appendix B

Polynomial Chaos Expansion for two dimensional Linear System

In order to fully demonstrate how the multivariate PC system is derived, the full integral solution for a two-dimensional problem is given. This is for an order of expansion, $n = 2$, and since there are two random variables i.e. $d = 2$, there are six PCE coefficients ($P = 6$). The subscript of each polynomial base corresponds to the multi-index and the notation has been shortened for the multivariate polynomial basis so that for e.g., $\psi_{10}(\xi) = \psi_1(\xi_1)\psi_0(\xi_2)$. Where $\psi_1(\xi_1)$ is the 1^{st} order univariate polynomial corresponding to the distribution of the parameter, whilst $\psi_0(\xi_2)$ is a univariate polynomial of order zero related to the distribution of the initial condition.

$$\dot{\mathbf{x}} = \begin{bmatrix} \dot{x}_0 \\ \dot{x}_1 \\ \dot{x}_2 \\ \dot{x}_3 \\ \dot{x}_4 \\ \dot{x}_5 \end{bmatrix} \begin{bmatrix} A_{00} & A_{01} & A_{02} & A_{03} & A_{04} & A_{05} \\ A_{10} & A_{11} & A_{12} & A_{13} & A_{14} & A_{15} \\ A_{20} & A_{21} & A_{22} & A_{23} & A_{24} & A_{25} \\ A_{30} & A_{31} & A_{32} & A_{33} & A_{34} & A_{35} \\ A_{40} & A_{41} & A_{42} & A_{43} & A_{44} & A_{45} \\ A_{50} & A_{51} & A_{52} & A_{53} & A_{54} & A_{55} \end{bmatrix} \begin{bmatrix} x_0 \\ x_1 \\ x_2 \\ x_3 \\ x_4 \\ x_5 \end{bmatrix} \tag{B.1}$$

where,

$$\dot{x}_0 \quad \text{terms} \quad \begin{cases} \gamma_0 &= < \psi_{00}^2(\xi) > \; = \int \psi_{00}(\xi)\psi_{00}(\xi) \\ A_{00} &= \frac{1}{\gamma_0}[a_0 \int \psi_{00}(\xi)\psi_{00}(\xi)\psi_{00}(\xi) + a_2 \int \psi_{01}(\xi)\psi_{00}(\xi)\psi_{00}(\xi)] \\ A_{01} &= \frac{1}{\gamma_0}[a_0 \int \psi_{00}(\xi)\psi_{10}(\xi)\psi_{00}(\xi) + a_2 \int \psi_{01}(\xi)\psi_{10}(\xi)\psi_{00}(\xi)] \\ A_{02} &= \frac{1}{\gamma_0}[a_0 \int \psi_{00}(\xi)\psi_{01}(\xi)\psi_{00}(\xi) + a_2 \int \psi_{01}(\xi)\psi_{01}(\xi)\psi_{00}(\xi)] \\ A_{03} &= \frac{1}{\gamma_0}[a_0 \int \psi_{00}(\xi)\psi_{20}(\xi)\psi_{00}(\xi) + a_2 \int \psi_{01}(\xi)\psi_{20}(\xi)\psi_{00}(\xi)] \\ A_{04} &= \frac{1}{\gamma_0}[a_0 \int \psi_{00}(\xi)\psi_{11}(\xi)\psi_{00}(\xi) + a_2 \int \psi_{01}(\xi)\psi_{11}(\xi)\psi_{00}(\xi)] \\ A_{05} &= \frac{1}{\gamma_0}[a_0 \int \psi_{00}(\xi)\psi_{02}(\xi)\psi_{00}(\xi) + a_2 \int \psi_{01}(\xi)\psi_{02}(\xi)\psi_{00}(\xi)] \end{cases} \tag{B.2}$$

$$\dot{x}_1 \quad \text{terms} \quad \begin{cases} \gamma_1 &= < \psi_{10}^2(\xi) > \; = \int \psi_{10}(\xi)\psi_{10}(\xi) \\ A_{10} &= \frac{1}{\gamma_1}[a_0 \int \psi_{00}(\xi)\psi_{00}(\xi)\psi_{10}(\xi) + a_2 \int \psi_{01}(\xi)\psi_{00}(\xi)\psi_{10}(\xi)] \\ A_{11} &= \frac{1}{\gamma_1}[a_0 \int \psi_{00}(\xi)\psi_{10}(\xi)\psi_{10}(\xi) + a_2 \int \psi_{01}(\xi)\psi_{10}(\xi)\psi_{10}(\xi)] \\ A_{12} &= \frac{1}{\gamma_1}[a_0 \int \psi_{00}(\xi)\psi_{01}(\xi)\psi_{10}(\xi) + a_2 \int \psi_{01}(\xi)\psi_{01}(\xi)\psi_{10}(\xi)] \\ A_{13} &= \frac{1}{\gamma_1}[a_0 \int \psi_{00}(\xi)\psi_{20}(\xi)\psi_{10}(\xi) + a_2 \int \psi_{01}(\xi)\psi_{20}(\xi)\psi_{10}(\xi)] \\ A_{14} &= \frac{1}{\gamma_1}[a_0 \int \psi_{00}(\xi)\psi_{11}(\xi)\psi_{10}(\xi) + a_2 \int \psi_{01}(\xi)\psi_{11}(\xi)\psi_{10}(\xi)] \\ A_{15} &= \frac{1}{\gamma_1}[a_0 \int \psi_{00}(\xi)\psi_{02}(\xi)\psi_{10}(\xi) + a_2 \int \psi_{01}(\xi)\psi_{02}(\xi)\psi_{10}(\xi)] \end{cases} \tag{B.3}$$

$$\dot{x}_2 \quad \text{terms} \quad \begin{cases} \gamma_2 & = & < \psi_{01}^2(\xi) > & = \int \psi_{01}(\xi)\psi_{01}(\xi) \\ A_{20} & = \frac{1}{\gamma_2}[a_0 \int \psi_{00}(\xi)\psi_{00}(\xi)\psi_{01}(\xi) + a_2 \int \psi_{01}(\xi)\psi_{00}(\xi)\psi_{01}(\xi)] \\ A_{21} & = \frac{1}{\gamma_2}[a_0 \int \psi_{00}(\xi)\psi_{10}(\xi)\psi_{01}(\xi) + a_2 \int \psi_{01}(\xi)\psi_{10}(\xi)\psi_{01}(\xi)] \\ A_{22} & = \frac{1}{\gamma_2}[a_0 \int \psi_{00}(\xi)\psi_{01}(\xi)\psi_{01}(\xi) + a_2 \int \psi_{01}(\xi)\psi_{01}(\xi)\psi_{01}(\xi)] \\ A_{23} & = \frac{1}{\gamma_2}[a_0 \int \psi_{00}(\xi)\psi_{20}(\xi)\psi_{01}(\xi) + a_2 \int \psi_{01}(\xi)\psi_{20}(\xi)\psi_{01}(\xi)] \\ A_{24} & = \frac{1}{\gamma_2}[a_0 \int \psi_{00}(\xi)\psi_{11}(\xi)\psi_{01}(\xi) + a_2 \int \psi_{01}(\xi)\psi_{11}(\xi)\psi_{01}(\xi)] \\ A_{25} & = \frac{1}{\gamma_2}[a_0 \int \psi_{00}(\xi)\psi_{02}(\xi)\psi_{01}(\xi) + a_2 \int \psi_{01}(\xi)\psi_{02}(\xi)\psi_{01}(\xi)] \end{cases} \tag{B.4}$$

$$\dot{x}_3 \quad \text{terms} \quad \begin{cases} \gamma_3 & = & < \psi_{20}^2(\xi) > & = \int \psi_{20}(\xi)\psi_{20}(\xi) \\ A_{30} & = \frac{1}{\gamma_3}[a_0 \int \psi_{00}(\xi)\psi_{00}(\xi)\psi_{20}(\xi) + a_2 \int \psi_{01}(\xi)\psi_{00}(\xi)\psi_{20}(\xi)] \\ A_{31} & = \frac{1}{\gamma_3}[a_0 \int \psi_{00}(\xi)\psi_{10}(\xi)\psi_{20}(\xi) + a_2 \int \psi_{01}(\xi)\psi_{10}(\xi)\psi_{20}(\xi)] \\ A_{32} & = \frac{1}{\gamma_3}[a_0 \int \psi_{00}(\xi)\psi_{01}(\xi)\psi_{20}(\xi) + a_2 \int \psi_{01}(\xi)\psi_{01}(\xi)\psi_{20}(\xi)] \\ A_{33} & = \frac{1}{\gamma_3}[a_0 \int \psi_{00}(\xi)\psi_{20}(\xi)\psi_{20}(\xi) + a_2 \int \psi_{01}(\xi)\psi_{20}(\xi)\psi_{20}(\xi)] \\ A_{34} & = \frac{1}{\gamma_3}[a_0 \int \psi_{00}(\xi)\psi_{11}(\xi)\psi_{20}(\xi) + a_2 \int \psi_{01}(\xi)\psi_{11}(\xi)\psi_{20}(\xi)] \\ A_{35} & = \frac{1}{\gamma_3}[a_0 \int \psi_{00}(\xi)\psi_{02}(\xi)\psi_{20}(\xi) + a_2 \int \psi_{01}(\xi)\psi_{02}(\xi)\psi_{20}(\xi)] \end{cases} \tag{B.5}$$

$$\dot{x}_4 \quad \text{terms} \quad \begin{cases} \gamma_4 & = & < \psi_{11}^2(\xi) > & = \int \psi_{11}(\xi)\psi_{11}(\xi) \\ A_{40} & = \frac{1}{\gamma_4}[a_0 \int \psi_{00}(\xi)\psi_{00}(\xi)\psi_{11}(\xi) + a_2 \int \psi_{01}(\xi)\psi_{00}(\xi)\psi_{11}(\xi)] \\ A_{41} & = \frac{1}{\gamma_4}[a_0 \int \psi_{00}(\xi)\psi_{10}(\xi)\psi_{11}(\xi) + a_2 \int \psi_{01}(\xi)\psi_{10}(\xi)\psi_{11}(\xi)] \\ A_{42} & = \frac{1}{\gamma_4}[a_0 \int \psi_{00}(\xi)\psi_{01}(\xi)\psi_{11}(\xi) + a_2 \int \psi_{01}(\xi)\psi_{01}(\xi)\psi_{11}(\xi)] \\ A_{43} & = \frac{1}{\gamma_4}[a_0 \int \psi_{00}(\xi)\psi_{20}(\xi)\psi_{11}(\xi) + a_2 \int \psi_{01}(\xi)\psi_{20}(\xi)\psi_{11}(\xi)] \\ A_{44} & = \frac{1}{\gamma_4}[a_0 \int \psi_{00}(\xi)\psi_{11}(\xi)\psi_{11}(\xi) + a_2 \int \psi_{01}(\xi)\psi_{11}(\xi)\psi_{11}(\xi)] \\ A_{45} & = \frac{1}{\gamma_4}[a_0 \int \psi_{00}(\xi)\psi_{02}(\xi)\psi_{11}(\xi) + a_2 \int \psi_{01}(\xi)\psi_{02}(\xi)\psi_{11}(\xi)] \end{cases} \tag{B.6}$$

$$\dot{x}_5 \quad \text{terms} \quad \begin{cases} \gamma_5 & = & < \psi_{02}^2(\xi) > & = \int \psi_{02}(\xi)\psi_{02}(\xi) \\ A_{50} & = \frac{1}{\gamma_5}[a_0 \int \psi_{00}(\xi)\psi_{00}(\xi)\psi_{02}(\xi) + a_2 \int \psi_{01}(\xi)\psi_{00}(\xi)\psi_{02}(\xi)] \\ A_{51} & = \frac{1}{\gamma_5}[a_0 \int \psi_{00}(\xi)\psi_{10}(\xi)\psi_{02}(\xi) + a_2 \int \psi_{01}(\xi)\psi_{10}(\xi)\psi_{02}(\xi)] \\ A_{52} & = \frac{1}{\gamma_5}[a_0 \int \psi_{00}(\xi)\psi_{01}(\xi)\psi_{02}(\xi) + a_2 \int \psi_{01}(\xi)\psi_{01}(\xi)\psi_{02}(\xi)] \\ A_{53} & = \frac{1}{\gamma_5}[a_0 \int \psi_{00}(\xi)\psi_{20}(\xi)\psi_{02}(\xi) + a_2 \int \psi_{01}(\xi)\psi_{20}(\xi)\psi_{02}(\xi)] \\ A_{54} & = \frac{1}{\gamma_5}[a_0 \int \psi_{00}(\xi)\psi_{11}(\xi)\psi_{02}(\xi) + a_2 \int \psi_{01}(\xi)\psi_{11}(\xi)\psi_{02}(\xi)] \\ A_{55} & = \frac{1}{\gamma_5}[a_0 \int \psi_{00}(\xi)\psi_{02}(\xi)\psi_{02}(\xi) + a_2 \int \psi_{01}(\xi)\psi_{02}(\xi)\psi_{02}(\xi)] \end{cases} \tag{B.7}$$

Here the integral terms corresponding to a zero initial PCE coefficient have been omitted for brevity. Due to the fact that $a_i = [\mu_a, 0, \sigma_a, 0, ..., 0]$, there are only two integral terms in each A matrix entry.

Bibliography

[1] NASA, "Entry, descent and landing," July 2017. Available at `https://mars.nasa.gov/msl/mission/technology/insituexploration/edl/`.

[2] T. J. Sullivan, *Introduction to Uncertainty Quantification*. Coventry, UK: Springer, 2015.

[3] N. Wiener, "The homogeneous chaos," *American Journal of Mathematics*, vol. 60, No. 4, pp. 897–936, 1938.

[4] D. Xiu, *Numerical methods for stochastic computations: a spectral method approach*. New Jersey, USA: Princeton University Press, 2010.

[5] R. G. Ghanem and P. Spanos, *Stochastic Finite Elements: a Spectral Approach*. New York, USA: Springer, 1991.

[6] D. Xiu and G. E. Karniadakis, "Modeling uncertainty in flow simulations via generalized polynomial chaos," *Journal of Computational Physics*, vol. 187, pp. 137–167, 2003.

[7] D. Xiu, "Fast numerical methods for stochastic computations: A review," *Communications in Computational Physics*, vol. 5, No.2, pp. 242–272, 2009.

[8] D. Xiu and G. E. Karniadakis, "The wiener askey polynomial chaos for stochastic differential equations," *Journal of Scientific Computing*, vol. 24, No. 2, pp. 619–644, 2002.

[9] D. Xiu and C. Lucor, "Stochastic modeling of flow-structure interactions using generalized polynomial chaos.," *Journal of Fluids Engineering*, vol. 124, pp. 51–59, 2002.

[10] O. P. Le Maitre and O. M. Knio, *Spectral methods for uncertainty quantification with application to computational fluid dynamics*. Springer, 2010.

[11] B. Debusschere et al, "Protein labeling reactions in electrochemical microchannel flow: Numerical simulation and uncertainty propagation," *Physics of Fluids*, vol. 15, No.8, pp. 2238–2250, 2003.

[12] B. Debusschere et al, "Numerical challenges in the use of polynomial chaos representations for stochastic processes," *Journal of Scientific Computing*, vol. 26, No.2, pp. 698–719, 2004.

[13] *Proc. 2010 IEEE International Symposium on Computer-Aided Control System Design*, Part of 2010 IEEE Multi-Conference on Systems and Control, (Tokyo, Japan), IEEE, 2010.

[14] F. S. Hoover, "Gradient dynamic optimization with legendre chaos," *Science Direct*, vol. 44, pp. 135–140, 2008.

[15] E. D. Blanchard, "A polynomial chaos-based kalman filter approach for parameter estimation of mechanical systems," *Journal of Dynamic Systems, Measurement and Control*, vol. 132, No.6, pp. 242–272, 2010.

[16] G. Kewlani et al, "A polynomial chaos approach to the analysis of vehicle dynamics under uncertainty," *Vehicle System Dynamics*, vol. 50, No.5, pp. 1–26, 2012.

[17] I. M. Ross, *A Primer on Pontryagin's Principle in Optimal Control*. Collegiate Publishers, 2015.

[18] M. Sagliano and S. Theil, "Hybrid jacobian computation for fast optimal trajectories generation," in *AIAA Guidance, Navigation, and Control Conference, Boston, USA,*, 2013.

[19] M. Sagliano, "Performance analysis of linear and nonlinear techniques for automatic scaling of discretized control problems," *Operations Research Letters, Vol.42 Issue 3, May 2014, pp. 213-216*, 2014.

[20] L. Huneker, M. Sagliano, and Y. Arslantas, "Spartan: An improved global pseudospectral algorithm for high-fidelity entry-descent-landing guidance analysis," in *30th International Symposium on Space Technology and Science, Kobe, Japan, 2015*, 2015.

[21] V. D'Onofrio, "Implementation of advanced differentiation methods for optimal trajectory computation," Master's thesis, University of Naples Federico II, Naples, 2015.

[22] M. Sagliano, S. Theil, V. D'Onofrio, and M. Bergsma, "Spartan: A novel pseudospectral algorithm for entry, descent, and landing analysis," in *4th CEAS Eurognc conference, Warsaw*, 2017.

[23] M. Sagliano, S. Theil, M. Bergsma, V. D'Onofrio, L. Whittle, and G. Viavattene, "On the radau pseudospectral method: theoretical and implementation advances," *CEAS SPACE Journal*, 2017.

[24] A. Prabhakar et al, "Polynomial chaos-based analysis of probabilistic uncertainty in hypersonic flight dynamics," *Journal of Guidance, Control, and Dynamics*, vol. 33, No.1, pp. 222–234, 2010.

[25] P. Dutta and R. Bhattachrya, "Non linear estimation of hypersonic flight using polynomial chaos," *Journal of Guidance, Control, and Dynamics*, vol. 33, No.6, pp. 1765–1778, 2010.

[26] J. Fisher and R. Bhattachrya, "Optimal trajectory generation with probabilistic system uncertainty using polynomial chaos," *Journal of Dynamic Systems, Measurement and Control*, vol. 133, pp. 1765–1778, 2011.

[27] F. Xiong, Y. Xiong, and B. Xue, "Trajectory optimization under uncertainty based on polynomial chaos expansion," in *Part of AIAA SciTech*, (Kissimmee, Florida USA), AIAA, 2014.

[28] F. Xiong, C. Shishi, and Y. Xiong, "Dynamic system uncertainty propagation using polynomial chaos," *Chinese Journal of Aeronautics*, vol. 27, No.5, pp. 1156–1170, 2015.

[29] P. Spanos and R. Ghanem, "Stochastic finite element expansion for random media," tech. rep., Department of Civil Engineering and Mechanical Engineering Rice University, 1988.

[30] F. Xiong and J. S. Hesthaven, "High order collocation methods for differential equations with random inputs," *Journal of Scientific Computing*, vol. 27, No.3, pp. 1118–1139, 2015.

[31] B. Chouvion and E. Sarrouy, "Development of error criteria for adaptive multi-element polynomial chaos approaches," *Mechanical Systems and Signal Processing*, vol. 66, pp. 201–222, 2016.

[32] X. Wan and G. Karniadakis, "An adaptive multi-element generalized polynomial chaos method for stochastic differential equations," *Journal of Computational Physics*, vol. 289, pp. 617–642, 2005.

[33] Wolfram Mathworld, "Inner product space," June 2017. Available at `http://mathworld.wolfram.com/InnerProductSpace.html`.

[34] G. Sansone, *Orthogonal Functions: Revised English Edition*. New York, USA: Dover, 1991.

[35] Wolfram Mathworld, "Cauchy sequence," June 2017. Available at `http://mathworld.wolfram.com/CauchySequence.html`.

[36] C. Heil, "Banach and hilbert space review," June 2017. Available at `http://people.math.gatech.edu/~heil/handouts/banach.pdf`.

[37] R. Askey, *Orthogonal Polynomials and Special Functions*. Society for Industrial and Applied Mathematics, Philadelphia, Pennsylvania, 1975.

[38] M. R. Spiegel and J. Liu, *Mathematical Handbook of formulas and tables*. Schaum's, 1999.

[39] T. Delft, "Recurrence relation," June 2017. Available at `https://homepage.tudelft.nl/11r49/documents/wi4006/orthopoly.pdf`.

[40] R. Z. Iqbal, *Computation of nodes and weights of Gaussian quadrature rule by using Jacobi's method*. PhD thesis, The University of Birmingham, 2008.

[41] K. L. Judd, "Quadrature methods," July 2017. Available at `http://ice.uchicago.edu/2012_presentations/Faculty/Judd/Quadrature_ICE11.pdf`.

[42] Wolfram Mathworld, "Hermite gauss quadrature," July 2017. Available at `http://mathworld.wolfram.com/Hermite-GaussQuadrature.html`.

[43] Wolfram Mathworld, "Normal distribution," July 2017. Available at `http://mathworld.wolfram.com/NormalDistribution.html`.

[44] R. H. Cameron and W. T. Martin, "The orthogonal development of non-linear functionals in a series of fourier-hermite functionals," *Annals of Mathematics*, vol. 48 No. 2, pp. 385–392, 1947.

[45] B. Sudret and A. Der Kiureghian, "Stochastic finite element methods and reliability," Tech. Rep. UCB/SEMM-2000/08, UC Berkeley, 2000.

[46] S. Streif, F. Petzke, A. Mesbah, R. Findeisen, and R. D. Braatz, "Optimal experimental design for probabilistic model discrimination using polynomial chaos," in *19th IFAC World Congress*, (Cape Town, South Africa), Aug 24-29, 2014.

[47] D. Garg, *Advances in Global Pseudospectral Methods for Optimal Control*. PhD thesis, University of Florida, Gainesville, 2011.

[48] A. V. Rao, "A survey of numerical methods for optimal control," in *AAS/AIAA Astrodynamics Specialist Conference, AAS Paper 09-334, Pittsburgh, PA, August 10 - 13*, 2009.

[49] K. Aykutlug and K. D. Mease, "Approximate solution of hyper-sensitive optimal control problems using finite-time lyapunov analysis," in *American Control Conference*, (St. Louis, MO, USA), 2009.

[50] S. Streif, F. Petzke, and R. Mesbah, "Polynomial chaos expansion toolbox for matlab," July 2015. Available at `https://www.tu-chemnitz.de/etit/control/research/PCET/index.php.en`.

[51] J. Leys and E. Ghys, "Chaos: Strange attractions," July 2017. Available at `http://www.chaos-math.org/en/chaos-vii-strange-attractors`.

[52] R. Bhattacharya, *Polynomial Chaos - Workshop on Uncertainty Analysis and Estimation*. Aerospace Engineering, Texas A M University., 2015.